Arbitrary-rate relaxation techniques for the numerical modeling of compressible two-phase flows with heat and mass transfer

Marica Pelanti*,[a]

[a] *IMSIA, UMR 9219 ENSTA-CNRS-EDF-CEA,*
ENSTA Paris - Institut Polytechnique de Paris,
828, Boulevard des Maréchaux, 91120 Palaiseau, France

Abstract

We describe compressible two-phase flows by a single-velocity six-equation flow model, which is composed of the phasic mass and total energy equations, one volume fraction equation, and the mixture momentum equation. The model contains relaxation source terms accounting for volume, heat and mass transfer. The equations are numerically solved via a fractional step algorithm, where we alternate between the solution of the homogeneous hyperbolic portion of the system via a HLLC-type wave propagation scheme, and the solution of a sequence of three systems of ordinary differential equations for the relaxation source terms driving the flow toward mechanical, thermal and chemical equilibrium. In the literature often numerical relaxation procedures are based on simplifying assumptions, namely simple equations of state, such as the stiffened gas one, and instantaneous relaxation processes. These simplifications of the flow physics might be inadequate for the description of the thermodynamical processes involved in various flow problems. In the present work we introduce new numerical relaxation techniques with two significant properties: the capability to describe heat and mass transfer processes of arbitrary relaxation time, and the applicability to a general equation of state. We show the effectiveness of the proposed methods by presenting several numerical experiments.

Key words: Multiphase compressible flows, relaxation processes, liquid-vapor phase transition, finite volume schemes, Riemann solvers.
2000 MSC: 65M08, 76T10

1. Introduction

The modeling of multifluid and multiphase flows has applications in numerous fields of science, largely in many sectors of engineering such as aerospace, naval and nuclear technologies. In the present work we are interested in the simulation of compressible multiphase flows that might involve shocks, interfaces, and phase transition processes. Examples of flows of interest are those occurring in underwater explosions [13], nuclear power plants, and fuel injection systems. We describe these flows by a hyperbolic single-velocity six-equation compressible two-phase flow model that we have first studied in [55], and which is a variant of

*Corresponding author. Tel.: +33 1 69 31 98 19; Fax: +33 1 69 31 99 97.
Email address: marica.pelanti@ensta-paris.fr (Marica Pelanti)

the six-equation model presented in [66]. We employ a diffuse-interface approach, cf. [64]. The model system is composed of the phasic mass and total energy equations for the two phases, one volume fraction equation, and the mixture momentum equation. The model contains mechanical, thermal and chemical relaxation source terms, accounting respectively for volume, heat and mass transfer. The considered model belongs to the class of Baer–Nunziato-type [4] multiphase compressible flow models. The seven-equation two-phase flow model of Baer–Nunziato [4] (and the variant of Saurel–Abgrall [60]) is the most general model able to account for velocity, pressure, temperature and chemical potential disequilibria between the phases. From this full non-equilibrium seven-equation model endowed with relaxation source terms a hierarchy of relaxed models can be established by considering combinations of infinite-rate relaxation processes driving the flow to different levels of equilibrium [44]. The six-equation model considered in the present work represents the relaxed velocity equilibrium model obtained from the seven-equation Baer–Nunziato model in the limit of instantaneous kinetic equilibrium. From the six-equation single-velocity model a sub-hierarchy of relaxed models can be then obtained [24, 45]. In the limit of instantaneous mechanical relaxation we obtain the five-equation pressure equilibrium model of Kapila *et al.* [31]. In the limit of instantaneous mechanical and thermal relaxation we obtain a four-equation pressure and temperature equilibrium two-phase model [46, 34, 61, 11, 20], and in the limit of full instantaneous thermodynamic equilibrium we obtain the three-equation Homogeneous Equilibrium Model (HEM) [73]. Let us note that the numerical solution method for the six-equation model must be able to approximate solutions of the relaxed models in the hierarchy when appropriate instantaneous relaxation processes are activated. We also recall a different four-equation two-phase flow model of the Baer–Nunziato class, the liquid-vapor Homogeneous Relaxation Model (HRM) with mass transfer of [7, 21], which does not enter in the aforementioned hierarchy. The thermodynamic closure of this model consists in the assumption of mechanical equilibrium and vapor phase at saturation, and the model accounts for thermal disequilibrium.

The considered class of models with relaxation source terms in the literature is classically solved numerically via a fractional step algorithm where one alternates between the solution of the homogeneous hyperbolic portion of the model system and the solution of a sequence of systems of ordinary differential equations for the relaxation source terms [60, 63, 66, 65, 74, 80, 46, 55, 14, 36, 59, 53, 40, 34, 61, 11, 9, 67, 68, 25]. We also adopt here this operator splitting approach for the numerical approximation of the six-equation model, and for the solution of the homogeneous system we employ a second-order accurate finite volume wave propagation scheme [43, 42] based on the HLLC-type Riemann solver that we have presented in [55] (and which later we have also re-interpreted as a Suliciu-type Riemann solver [19]).

For the numerical approximation of the mechanical, thermal and chemical relaxation processes often in the literature it is assumed that these processes are instantaneous [66, 65, 80, 36, 59, 34, 61, 11, 14, 68], and this assumption was also made in our previous six-equation numerical model [55, 53]. This simplifying hypothesis is advantageous because in this case one does not need to solve the system of ordinary differential equations that govern the relaxation process, but it suffices to impose equilibrium conditions to obtain a system of algebraic equations to be solved for the unknown relaxed equilibrium state. The assumption of instantaneous mechanical equilibrium can be indeed considered appropriate for the flows of interest (see also for instance the discussion on characteristic relaxation scales in [31]). On the other hand, the hypothesis of instantaneous thermo-chemical relaxation might be inadequate for the description of the thermodynamical processes involved in several flow problems. For instance, in some transient phenomena such as fast depressurizations the delay of vaporization and the appearance

of metastable states are key features in the flow evolution, and they can be described only by models that account for non-instantaneous mass transfer, such as those in [21, 22, 46, 16]. Another simplification often considered in the literature is the choice of a simple equation of state, the stiffened gas equation of state [66, 65, 80, 36, 59, 34, 14, 9, 67, 68], which results from a linearization of the more general Mie–Grüneisen pressure law [48]. The stiffened gas equation of state is very convenient for numerical purposes, however it might not allow an accurate flow characterization over a wide temperature range, and in particular for liquid-vapor flows it might not provide a precise estimation of the saturation conditions [35]. Some more recent multiphase numerical models for liquid-vapor flows adopt a slightly more accurate equation of state, the Noble–Abel stiffened gas equation of state [37, 61, 11, 25], and few models adopt complex and very precise equations of state such as the IAPWS Industrial Formulation 1997 for Water and Steam [77], which we have used in previous work [16, 17, 18].

One main objective of the present work is to develop new relaxation techniques for heat and mass transfer capable to model processes of any relaxation rate, both instantaneous infinite-rate processes and slow finite-rate ones. We are primarily interested in arbitrary-rate mass transfer and the capability to model metastable states in vapor-liquid flows with phase transition. Another objective is the design of relaxation techniques efficiently applicable to a general equation of state. A known difficulty encountered in the numerical solution of a system of ordinary differential equations with a relaxation source term is the stiffness of the problem in case of nearly instantaneous relaxation, which would require computationally expensive implicit time integration techniques. Our idea consists in describing the relaxation processes by systems of ordinary differential equations obtained from the governing two-phase equations that admit analytical semi-exact exponential solutions. Similar approaches using exponential solutions to solve stiff relaxation systems were used for instance in [21, 28, 54, 3, 16, 17]. Let us remark some differences with respect to our previous work [17, 18] on relaxation techniques for non-instantaneous heat and mass transfers and general equation of state. The principal thermal and chemical relaxation procedures proposed in [17, 18] were based on relaxation systems derived from physical principles solved numerically via explicit Runge–Kutta methods with adaptive step size. These explicit methods were not suited for stiff problems, and the employment of implicit solvers was found too computationally expensive, thus the procedures were not adequate for stiff instantaneous or nearly instantaneous processes. To solve problems with infinite-rate transfers alternative techniques based on exponential solutions were briefly proposed in the Appendix of [17]. Nonetheless these techniques were specifically aimed at the limit case of infinitely fast relaxation and built differently with respect to the procedures of the present work. In particular it was assumed *a priori* an exponential decay of the pressure, temperature and chemical potential differences, whereas in the present work the relaxation systems with exponential solution are obtained from the equations of the two-phase parent and relaxed models after assuming some quantities constant during the relaxation process.

The relaxation procedures developed here results to be simple, robust and effective, and by construction they can be also used for other two-phase models belonging to the hierarchy established from the Baer–Nunziato model. Moreover, the techniques guarantee consistency of the values of the relaxed states with the mixture pressure law, so that the numerical method is mixture-energy-consistent in the sense defined in [55].

This article is structured as follows. In Section 2 we present the six-equation two-phase flow model under study. In Section 3 we recall the hierarchy of relaxed models established from the parent six-equation model. Examples of equations of state to close the model systems used in the numerical experiments are reported in Section 4. In Section 5 we outline the fractional step

method employed to solve the two-phase equations. In Section 6 we recall the wave-propagation scheme used for the solution of the homogeneous system, and we detail then in Section 7 the new relaxation techniques to treat the phase transfer source terms. Numerical experiments are finally presented in Section 8, including tests with shocks, interfaces, evaporation waves and metastable states.

2. Single-velocity six-equation two-phase compressible flow model

We consider a compressible flow composed of two phases that we assume in kinetic equilibrium with velocity $\vec{u}$. The volume fraction, density, pressure, specific internal energy of each phase will be denoted by α_k, ρ_k, p_k, ε_k, $k = 1, 2$, respectively. We will denote the phasic internal energy per unit volume with $\mathcal{E}_k = \rho_k \varepsilon_k$, and the phasic total energy per unit volume with $E_k = \mathcal{E}_k + \rho_k \frac{|\vec{u}|^2}{2}$. The saturation condition is $\alpha_1 + \alpha_2 = 1$. The mixture density is $\rho = \sum_{k=1}^{2} \alpha_k \rho_k$, the mixture internal energy per unit volume $\mathcal{E} = \sum_{k=1}^{2} \alpha_k \mathcal{E}_k$, and the mixture total energy $E = \sum_{k=1}^{2} \alpha_k E_k$. The nomenclature of the variables is summarized in Table 1. We describe the two-phase flow by the following system [55] consisting of $5 + d$ equations, where d denotes the spatial dimension:

$$\partial_t \alpha_1 + \vec{u} \cdot \nabla \alpha_1 = \mathcal{P}, \tag{1a}$$

$$\partial_t (\alpha_1 \rho_1) + \nabla \cdot (\alpha_1 \rho_1 \vec{u}) = \mathcal{M}, \tag{1b}$$

$$\partial_t (\alpha_2 \rho_2) + \nabla \cdot (\alpha_2 \rho_2 \vec{u}) = -\mathcal{M}, \tag{1c}$$

$$\partial_t (\rho \vec{u}) + \nabla \cdot (\rho \vec{u} \otimes \vec{u} + (\alpha_1 p_1 + \alpha_2 p_2) \mathbb{I}) = 0, \tag{1d}$$

$$\partial_t (\alpha_1 E_1) + \nabla \cdot (\alpha_1 (E_1 + p_1) \vec{u}) + \Sigma = -p_1 \mathcal{P} + \mathcal{Q} + \left(g_\mathrm{I} + \tfrac{|\vec{u}|^2}{2} \right) \mathcal{M}, \tag{1e}$$

$$\partial_t (\alpha_2 E_2) + \nabla \cdot (\alpha_2 (E_2 + p_2) \vec{u}) - \Sigma = p_\mathrm{I} \mathcal{P} - \mathcal{Q} - \left(g_\mathrm{I} + \tfrac{|\vec{u}|^2}{2} \right) \mathcal{M}, \tag{1f}$$

where the non-conservative term Σ appearing in the phasic total energy equations is given by

$$\Sigma = -\vec{u} \cdot \vec{\Xi}, \qquad \vec{\Xi} = Y_2 \nabla (\alpha_1 p_1) - Y_1 \nabla (\alpha_2 p_2). \tag{1g}$$

Here $Y_k = \frac{\alpha_k \rho_k}{\rho}$ is the mass fraction of phase k. Above we have denoted with $\mathcal{P}$, $\mathcal{Q}$ and $\mathcal{M}$ the volume, heat and mass transfer terms between the two phases. These transfer terms are expressed as relaxation terms:

$$\mathcal{P} = \mu (p_1 - p_2), \quad \mathcal{Q} = \vartheta (T_2 - T_1), \quad \mathcal{M} = \nu (g_2 - g_1), \tag{2}$$

where T_k denotes the phasic temperature, and g_k the phasic chemical potential. $\mu \geq 0$, $\vartheta \geq 0$, $\nu \geq 0$ are parameters or more generally functions expressing the rate of mechanical, thermal and chemical relaxation, respectively. Here we are interested in modeling flows in mechanical equilibrium, hence we will always consider that mechanical relaxation is an instantaneous process, thus we assume $\mu \to +\infty$. Indeed, following the same idea of [65, 66, 55], the parent non-equilibrium two-phase flow model with instantaneous pressure relaxation (1) is used to approximate solutions to the limiting pressure-equilibrium flow model (see model (9) in section 3.1), which is the physical flow model of interest. Concerning thermal and chemical relaxation, in contrast to [65, 55], no specific assumption is made for the heat and mass transfer rate, and hence for ϑ and ν (provided ϑ, $\nu \geq 0$). The quantity p_I is an interface pressure and g_I is an

interface chemical potential. The definition of the relaxation parameters or functions and of the interface quantities needs to be consistent with the second law on thermodynamics, namely the entropy production for the mixture must be positive. Sufficient conditions are (see proof in [24]) $\mu,\ \vartheta,\ \nu \geq 0$ and

$$p_{\mathrm{I}} \in \{\min(p_1, p_2), \max(p_1, p_2)\}, \quad g_{\mathrm{I}} \in \{\min(g_1, g_2), \max(g_1, g_2)\}. \tag{3}$$

Hence, it suffices to define the interface quantities p_{I} and g_{I} as convex combinations of the respective phasic quantities. Concerning p_{I}, for our numerical tests we have used the definition proposed in [62, 66], which we already used in [55]: $p_{\mathrm{I}} = \frac{Z_2^a p_1 + Z_1^a p_2}{Z_1^a + Z_2^a}$, where $Z_k^a = \rho_k c_k$ is the acoustic impedance of phase k. Other definitions are possible, for instance the one suggested in [60], $p_{\mathrm{I}} = \alpha_1 p_1 + \alpha_2 p_2$. Concerning g_{I}, we will see that we do not need to define it in our numerical scheme. To close the model system an equation of state for each phase must be provided, for instance through the specification of the pressure relations $p_k(\mathcal{E}_k, \rho_k)$ and the temperature relations $T_k(p_k, \rho_k)$. If thermo-chemical transfer terms are not considered, then the specification of the pressure laws $p_k(\mathcal{E}_k, \rho_k)$ (incomplete equation of state) suffices to solve the model system.

The two-phase model above is hyperbolic and the eigenvalues associated to the direction $\vec{n}$ are given by $\lambda_{1,5+d} = \vec{u}\cdot\vec{n} \mp c_{\mathrm{f}}\,,\ \lambda_l = \vec{u}\cdot\vec{n}$, for $l = 2, \ldots, 4+d$ (eigenvalue of multiplicity $3+d$). Here c_{f} is the non-equilibrium (frozen) speed of sound, given by

$$c_{\mathrm{f}} = \sqrt{Y_1 c_1^2 + Y_2 c_2^2}\,, \tag{4}$$

where $c_k\,,\ k = 1, 2$, is the speed of sound of phase k, which can be expressed as:

$$c_k = \sqrt{\Gamma_k h_k + \chi_k}\,, \tag{5}$$

where $h_k = (\mathcal{E}_k + p_k)/\rho_k$ is the specific enthalpy of phase k, and

$$\Gamma_k = \left(\frac{\partial p_k}{\partial \mathcal{E}_k}\right)_{\rho_k}, \qquad \chi_k = \left(\frac{\partial p_k}{\partial \rho_k}\right)_{\mathcal{E}_k}. \tag{6}$$

Note that the sum of the phasic total energy equations recovers a conservation law for the mixture total energy $E = \sum_{k=1}^{2} \alpha_k E_k$:

$$\partial_t E + \nabla\cdot(E\vec{u} + (\alpha_1 p_1 + \alpha_2 p_2)\vec{u}) = 0\,. \tag{7}$$

For later use, let us also write here the equations for the phasic pressures:

$$\partial_t p_k + \vec{u}\cdot\nabla p_k + \rho_k c_k^2 \nabla\cdot\vec{u} = \frac{(-1)^{k-1}}{\alpha_k}\left\{-[\Gamma_k(\mathcal{E}_k + p_{\mathrm{I}}) + \chi_k\rho_k]\mathcal{P} + \Gamma_k \mathcal{Q} + (\Gamma_k g_{\mathrm{I}} + \chi_k)\mathcal{M}\right\},\ k = 1, 2. \tag{8}$$

3. Hierarchy of single-velocity relaxed two-phase flow models

From the parent six-equation non-equilibrium model (1) presented in the previous section we can establish a hierarchy of hyperbolic relaxed single-phase two-phase flow models by considering the limit of combinations of instantaneous relaxation processes, see [24, 45]. The p-relaxed and pT-relaxed model equations recalled below will be used in the construction of the relaxation procedures in Section 7.2.

ρ_k = phasic density

α_k = volume fraction of phase k ($\alpha_1 + \alpha_2 = 1$)

$\vec{u}$ = velocity vector

ε_k = phasic specific internal energy

$\mathcal{E}_k = \rho_k \varepsilon_k$ = phasic internal energy per unit volume

$E_k = \mathcal{E}_k + \rho_k \frac{|\vec{u}|^2}{2}$ = phasic total energy per unit volume

p_k = phasic pressure

$p_\mathrm{m} = \alpha_1 p_1 + \alpha_2 p_2$

p = mixture equilibrium pressure

p_I = interface pressure

$\rho = \alpha_1\rho_1 + \alpha_2\rho_2$ = mixture density

$Y_k = \frac{\alpha_k \rho_k}{\rho}$ = mass fraction of phase k ($Y_1 + Y_2 = 1$)

$\varepsilon = Y_1\varepsilon_1 + Y_2\varepsilon_2$ = mixture specific internal energy

$\mathcal{E} = \rho\varepsilon = \alpha_1\mathcal{E}_1 + \alpha_2\mathcal{E}_2$ = mixture internal energy per unit volume

$E = \mathcal{E} + \frac{1}{2}\rho|\vec{u}|^2 = \alpha_1 E_1 + \alpha_2 E_2$ = mixture total energy per unit volume

$h_k = \frac{\mathcal{E}_k + p_k}{\rho_k}$ = phasic specific enthalpy

$h = Y_1 h_1 + Y_2 h_2$ = mixture specific enthalpy

$c_k = \sqrt{\left(\frac{\partial p_k}{\partial \rho_k}\right)_{s_k}}$ = sound speed of phase k

$c_\mathrm{f} = \sqrt{Y_1 c_1^2 + Y_2 c_2^2}$ = non-equilibrium (frozen) mixture sound speed

T_k = phasic temperature

T = mixture equilibrium temperature

s_k = phasic entropy

$s = Y_1 s_1 + Y_2 s_2$ = mixture entropy

g_k = phasic chemical potential

g_I = interface chemical potential

$\Gamma_k = \left(\frac{\partial p_k}{\partial \mathcal{E}_k}\right)_{\rho_k}$ = Grüneisen coefficient of phase k

$\chi_k = \left(\frac{\partial p_k}{\partial \rho_k}\right)_{\mathcal{E}_k}$

$\phi_k = \left(\frac{\partial \rho_k}{\partial T_k}\right)_{p_k} = -\rho_k\beta_k, \quad \beta_k$ = phasic coefficient of thermal expansion

$\zeta_k = \left(\frac{\partial \rho_k}{\partial p_k}\right)_{T_k} = \rho_k\mathcal{K}_{Tk}, \quad \mathcal{K}_{Tk}$ = phasic isothermal compressibility

$\mathcal{K}_{Sk} = \frac{1}{\rho_k c_k^2}$ = phasic isentropic compressibility

$\kappa_{pk} = T_k\left(\frac{\partial s_k}{\partial T_k}\right)_{p_k} = \left(\frac{\partial h_k}{\partial T_k}\right)_{p_k}$ =specific heat capacity at constant pressure

$\kappa_{vk} = T_k\left(\frac{\partial s_k}{\partial T_k}\right)_{\rho_k} = \left(\frac{\partial \varepsilon_k}{\partial T_k}\right)_{\rho_k}$ =specific heat capacity at constant volume

$C_{pk} = \alpha_k\rho_k\kappa_{pk}$ = phasic extensive heat capacity at constant pressure

Table 1: Nomenclature of variables.

3.1. Five-equation p-relaxed two-phase flow model

We assume that the flow is driven instantaneously to mechanical equilibrium, $p_1 = p_2 = p$, hence we consider $\mu \to +\infty$. The p-relaxed (pressure equilibrium) model, corresponding to the well known Kapila *et al.* model [31] (see also [49]), consists of $4 + d$ equations:

$$\partial_t \alpha_1 + \vec{u} \cdot \nabla \alpha_1 - \tfrac{\alpha_1 \alpha_2}{D}(\rho_2 c_2^2 - \rho_1 c_1^2)\nabla \cdot \vec{u} = \tfrac{1}{D}\left(\alpha_2 \Gamma_1 + \alpha_1 \Gamma_2\right)\mathcal{Q} + \tfrac{1}{D}\left(\alpha_2 \omega_{I1} + \alpha_1 \omega_{I2}\right)\mathcal{M}, \quad (9a)$$

$$\partial_t(\alpha_1 \rho_1) + \nabla \cdot (\alpha_1 \rho_1 \vec{u}) = \mathcal{M}, \quad (9b)$$

$$\partial_t(\alpha_2 \rho_2) + \nabla \cdot (\alpha_2 \rho_2 \vec{u}) = -\mathcal{M}, \quad (9c)$$

$$\partial_t(\rho \vec{u}) + \nabla \cdot (\rho \vec{u} \otimes \vec{u} + p\mathbb{I}) = 0, \quad (9d)$$

$$\partial_t E + \nabla \cdot ((E + p)\vec{u}) = 0, \quad (9e)$$

where

$$D = \alpha_1 \rho_2 c_2^2 + \alpha_2 \rho_1 c_1^2 \quad (10)$$

and

$$\omega_{Ik} = \Gamma_k(g_1 - h_k) + c_k^2 = \Gamma_k g_1 + \chi_k, \quad k = 1, 2. \quad (11)$$

The derivation of the above p-relaxed system from the parent system (1) is detailed in Appendix A, and it has been also illustrated in our work [56] for a more general N-phase model. Given the phasic energy laws $\mathcal{E}_k(p_k, \rho_k)$, the mixture pressure law $p = p(\mathcal{E}, \rho_1, \rho_2, \alpha_1)$ for this model is determined by the mixture energy relation

$$\mathcal{E} = \alpha_1 \mathcal{E}_1(p, \rho_1) + \alpha_2 \mathcal{E}_2(p, \rho_2), \quad (12)$$

where we have used the isobaric condition $p_1 = p_2 = p$. The speed of sound associated to the model is given by the well known Wood's speed of sound

$$c_p = \left(\rho \sum_{k=1}^{2} \frac{\alpha_k}{\rho_k c_k^2}\right)^{-\frac{1}{2}}. \quad (13)$$

Note that the term D (10) can be written in terms of c_p, $\frac{1}{D} = \frac{\rho c_p^2}{\rho_1 c_1^2 \rho_2 c_2^2}$. The pressure equation is:

$$\partial_t p + \vec{u} \cdot \nabla p + \rho c_p^2 \nabla \cdot \vec{u} = \tfrac{1}{D}\left[(\Gamma_1 \rho_2 c_2^2 - \Gamma_2 \rho_1 c_1^2)\mathcal{Q} + (\rho_2 c_2^2 \omega_{I1} - \rho_1 c_1^2 \omega_{I2})\mathcal{M}\right]. \quad (14)$$

Let us now write the equations for the phasic temperatures T_k, $k = 1, 2$, which we will use in the following:

$$\begin{aligned} &\partial_t T_k + \vec{u} \cdot \nabla T_k + \frac{\rho c_p^2}{\phi_k}\left(-\zeta_k + \frac{1}{c_k^2}\right)\nabla \cdot \vec{u} \\ &= \frac{1}{\phi_k D}\left[(-1)^k \frac{\rho_k}{\alpha_k}\left(\alpha_2 \Gamma_1 + \alpha_1 \Gamma_2\right) - \zeta_k(\Gamma_1 \rho_2 c_2^2 - \Gamma_2 \rho_1 c_1^2)\right]\mathcal{Q} \\ &+ \frac{1}{\phi_k}\left\{\frac{(-1)^{k-1}}{\alpha_k} + \frac{1}{D}\left[(-1)^k \frac{\rho_k}{\alpha_k}(\alpha_2 \omega_{I1} + \alpha_1 \omega_{I2}) - \zeta_k(\rho_2 c_2^2 \omega_{I1} - \rho_1 c_1^2 \omega_{I2})\right]\right\}\mathcal{M}, \end{aligned} \quad (15)$$

where we have introduced the derivatives

$$\phi_k = \left(\frac{\partial \rho_k}{\partial T_k}\right)_{p_k} = -\rho_k \beta_k \quad \text{and} \quad \zeta_k = \left(\frac{\partial \rho_k}{\partial p_k}\right)_{T_k} = \rho_k \mathcal{K}_{Tk}, \quad (16)$$

where β_k denotes the coefficient of thermal expansion and $\mathcal{K}_{Tk}$ the isothermal compressibility. Note also that we have the relations:

$$\beta_k = \frac{\Gamma_k \kappa_{pk}}{c_k^2} = \frac{\Gamma_k C_{pk}}{c_k^2 \alpha_k \rho_k} \quad \text{and} \quad \mathcal{K}_{Tk} = \mathcal{K}_{Sk} + \frac{\beta_k^2 T_k}{\rho_k \kappa_{pk}} = \frac{1}{\rho_k c_k^2} + \frac{\beta_k^2 T_k \alpha_k}{C_{pk}}, \tag{17}$$

where $\mathcal{K}_{Sk} = \frac{1}{\rho_k c_k^2}$ is the isentropic compressibility, and where $C_{pk} = \alpha_k \rho_k \kappa_{pk}$ and $\kappa_{pk} = \frac{\partial h_k}{\partial T_k}\Big|_{p_k} = T_k \frac{\partial s_k}{\partial T_k}\Big|_{p_k}$.

3.2. Four-equation pT-relaxed two-phase flow model

We now assume that the flow is driven instantaneously to both mechanical and thermal equilibrium, $p_1 = p_2 = p$, $T_1 = T_2 = T$. Hence we consider the limit $\mu \to +\infty$ and $\vartheta \to +\infty$. We obtain the following reduced model composed of $3 + d$ equations (used for instance in [46, 34, 61, 11, 20]):

$$\partial_t(\alpha_1\rho_1) + \nabla \cdot (\alpha_1\rho_1\vec{u}) = \mathcal{M}, \tag{18a}$$

$$\partial_t(\alpha_2\rho_2) + \nabla \cdot (\alpha_2\rho_2\vec{u}) = -\mathcal{M}, \tag{18b}$$

$$\partial_t(\rho\vec{u}) + \nabla \cdot (\rho\vec{u} \otimes \vec{u} + p\mathbb{I}) = 0, \tag{18c}$$

$$\partial_t E + \nabla \cdot ((E + p)\vec{u}) = 0. \tag{18d}$$

The mixture pressure law $p = p(\mathcal{E}, \rho_1, \rho_2)$ is determined by the energy relation (12), together with the isothermal condition $T_1(p, \rho_1) = T_2(p, \rho_2)$. The speed of sound for this model is given by

$$\frac{1}{c_{pT}^2} = \frac{1}{c_p^2} + \frac{\rho T C_{p1} C_{p2}}{C_{p1} + C_{p2}} \left(\frac{\Gamma_2}{\rho_2 c_2^2} - \frac{\Gamma_1}{\rho_1 c_1^2} \right)^2, \tag{19}$$

where we recall $C_{pk} = \alpha_k \rho_k \kappa_{pk}$ (extensive heat capacities). Let us finally write also the equations for the volume fraction α_1, the temperature T and the pressure p:

$$\partial_t \alpha_1 + \vec{u} \cdot \nabla\alpha_1 + \rho c_{pT}^2 \left[\alpha_1\alpha_2 \left(\frac{1}{\rho_2 c_2^2} - \frac{1}{\rho_1 c_1^2} \right) + \frac{T C_{p1} C_{p2}}{C_{p1} + C_{p2}} \left(\frac{\Gamma_2}{\rho_2 c_2^2} - \frac{\Gamma_1}{\rho_1 c_1^2} \right) \left(\frac{\alpha_1\Gamma_2}{\rho_2 c_2^2} + \frac{\alpha_2\Gamma_1}{\rho_1 c_1^2} \right) \right] \nabla \cdot \vec{u} = \mathcal{M}\mathcal{S}_\alpha, \tag{20}$$

$$\partial_t T + \vec{u} \cdot \nabla T + \frac{\rho c_{pT}^2 T}{C_{p1} + C_{p2}} \left(\frac{C_{p1}\Gamma_1}{\rho_1 c_1^2} + \frac{C_{p2}\Gamma_2}{\rho_2 c_2^2} \right) \nabla \cdot \vec{u} = \mathcal{M}\mathcal{S}_T, \tag{21}$$

$$\partial_t p + \vec{u} \cdot \nabla p + \rho c_{pT}^2 \nabla \cdot \vec{u} = \mathcal{M}\mathcal{S}_p, \tag{22}$$

where

$$\mathcal{S}_\alpha = \frac{1}{D_T} \left[\left(\frac{\alpha_1}{\Gamma_1} + \frac{\alpha_2}{\Gamma_2} \right) (\alpha_1\phi_1 + \alpha_2\phi_2) + \alpha_1\alpha_2 \left(\frac{\chi_1}{\Gamma_1} - \frac{\chi_2}{\Gamma_2} \right) (\phi_1\zeta_2 - \phi_2\zeta_1) \right], \tag{23a}$$

$$\mathcal{S}_T = \frac{1}{D_T} \left[\left(\frac{\chi_2}{\Gamma_2} - \frac{\chi_1}{\Gamma_1} \right) (\alpha_1\zeta_1\rho_2 + \alpha_2\zeta_2\rho_1) + \left(\frac{\rho_1 c_1^2}{\Gamma_1} - \frac{\rho_2 c_2^2}{\Gamma_2} \right) (\alpha_1\zeta_1 + \alpha_2\zeta_2) + \left(\frac{\alpha_1}{\Gamma_1} + \frac{\alpha_2}{\Gamma_2} \right) (\rho_2 - \rho_1) \right], \tag{23b}$$

$$\mathcal{S}_p = \frac{1}{D_T} \left[\left(\frac{\chi_1}{\Gamma_1} - \frac{\chi_2}{\Gamma_2} \right) (\alpha_1\phi_1\rho_2 + \alpha_2\phi_2\rho_1) + \left(\frac{\rho_2 c_2^2}{\Gamma_2} - \frac{\rho_1 c_1^2}{\Gamma_1} \right) (\alpha_1\phi_1 + \alpha_2\phi_2) \right], \tag{23c}$$

with

$$D_T = \alpha_1\alpha_2\left(\frac{\rho_1 c_1^2}{\Gamma_1} - \frac{\rho_2 c_2^2}{\Gamma_2}\right)(\phi_1\zeta_2 - \phi_2\zeta_1) + \left(\frac{\alpha_1}{\Gamma_1} + \frac{\alpha_2}{\Gamma_2}\right)(\alpha_1\phi_1\rho_2 + \alpha_2\phi_2\rho_1)\,. \tag{23d}$$

The derivation of these expressions of $\mathcal{S}_\alpha$, $\mathcal{S}_T$, $\mathcal{S}_p$ will be illustrated in Appendix B.

3.3. Three-equation pTg-relaxed two-phase flow model

For completeness, we also recall the relaxed model obtained by assuming full thermodynamic equilibrium, $p_1 = p_2 = p$, $T_1 = T_2 = T$, and $g_1 = g_2$. Hence we consider the limit $\mu \to +\infty$, $\vartheta \to +\infty$, and $\nu \to +\infty$. We obtain the homogeneous equilibrium model (HEM) composed of $2 + d$ equations (see e.g. [73, 12, 16, 26]):

$$\partial_t\rho + \nabla\cdot(\rho\vec{u}) = 0\,, \tag{24a}$$

$$\partial_t(\rho\vec{u}) + \nabla\cdot(\rho\vec{u}\otimes\vec{u} + p\mathbb{I}) = 0\,, \tag{24b}$$

$$\partial_t E + \nabla\cdot((E+p)\vec{u}) = 0\,. \tag{24c}$$

The mixture pressure law $p = p(\mathcal{E},\rho)$ is determined by the energy relation (12), the isothermal condition $T_1(p,\rho_1) = T_2(p,\rho_2)$, and the equilibrium condition $g_1(p,T) = g_2(p,T)$. The speed of sound is given by (see e.g. the systematic derivation of the speeds of sound of the various models in the hierarchy in [56])

$$\frac{1}{c_{pTg}^2} = \frac{1}{c_{pT}^2} + \frac{\rho T}{C_{p1}+C_{p2}}\left[\frac{\Gamma_1 C_{p1}}{\rho_1 c_1^2} + \frac{\Gamma_2 C_{p2}}{\rho_2 c_2^2} - \frac{1}{T}\left(\frac{dT}{dp}\right)_{\text{sat}}(C_{p1}+C_{p2})\right]^2. \tag{25}$$

We remark that subcharacteristic conditions hold for the speeds of sound of the two-phase flow models in the hierarchy [24]:

$$c_{pTg} \le c_{pT} \le c_p \le c_{\text{f}}\,. \tag{26}$$

The speed of sound is reduced whenever an additional equilibrium assumption is introduced.

4. Equation of State (EOS)

As indicated in Section 2 for the solution of the six-equation model (1) an equation of state must be specified for each phase. Let us note that in the numerical model we require that the two phases are both always present and a region of a pure phase k is approximated by a mixture with volume fraction $\alpha_k = 1 - \epsilon$, where $0 < \epsilon \ll 1$ is a small tolerance. For this reason, the equation of state of each phase must have a domain of validity that covers the entire thermodynamic domain of the problem of interest. The numerical techniques that we will present in the following sections can be employed for any choice of the equations of state for the two phases, provided each EOS in the considered domain has physically admissible states, ρ_k, $\mathcal{E}_k > 0$, and it satisfies the thermodynamic constraints $\kappa_{vk} = T_k\left(\frac{\partial s_k}{\partial T_k}\right)_{\rho_k} > 0$ and $\left(\frac{\partial p}{\partial v}\right)_{T_k} < 0$, $v = 1/\rho$. For the numerical experiments in the present work we will consider two particular equations of state, which can both be written in the form of the Mie–Grüneisen equation of state recalled hereafter. Let us remark that in several applications with phase change liquid and vapor of a species are described by a single equation of state, such as cubic equations of state like the Peng–Robinson EOS [57], or accurate multi-parameter equations of state such as the GERG-2008 EOS [33] or the IAPWS-IF97 EOS [77]. A single EOS of this type could be employed in the present numerical model only

for problems for which the thermodynamic domain is covered by the two-phase mixture domain of these equations, since in this domain an equation of state for each phase can be constructed (see e.g. [18]). We also note that the single liquid-vapor equations of state exhibit an inadmissible region of thermodynamic instability (the region of the saturation dome between the two spinodal curves), this limiting the domain of applicability. In contrast, the approach used in the present work that models phase change as a kinetic transformation does not present unstable regions (we refer to the detailed discussion in [66]).

4.1. Mie–Grüneisen equation of state

The incomplete Mie–Grüneisen equation of state has the form (see e.g. [48]):

$$p(\mathcal{E},\rho) = \Gamma(\rho)(\mathcal{E} - \rho\varepsilon_{\mathrm{r}}(\rho)) + p_{\mathrm{r}}(\rho)\,, \tag{27}$$

where $\Gamma(\rho)$ is the Grüneisen coefficient defined for a general EOS as in (6), and $\varepsilon_{\mathrm{r}}(\rho)$, $p_{\mathrm{r}}(\rho)$ are reference specific energy and pressure functions, respectively. An extension of this incomplete EOS to a complete one can be found in [47]. Many equations of state can be written in the form (27), including the JWL and NASG equations of state reported below.

For two-phase flows in mechanical equilibrium where each phase is governed by an equation of state with the form of the Mie-Grüneisen EOS, it is possible to obtain an explicit expression for the mixture pressure law (12):

$$p(\mathcal{E},\rho_1,\rho_2,\alpha_1) = \frac{\mathcal{E} - (\alpha_1\rho_1\varepsilon_{\mathrm{r}1}(\rho_1) + \alpha_2\rho_2\varepsilon_{\mathrm{r}2}(\rho_2)) + \left(\alpha_1\frac{p_{\mathrm{r}1}(\rho_1)}{\Gamma_1(\rho_1)} + \alpha_2\frac{p_{\mathrm{r}2}(\rho_2)}{\Gamma_2(\rho_2)}\right)}{\frac{\alpha_1}{\Gamma_1(\rho_1)} + \frac{\alpha_2}{\Gamma_2(\rho_2)}}. \tag{28}$$

This is an important advantage from the numerical point of view, since solving an implicit equation for the pressure can be computationally expensive.

4.2. Jones–Wilkins–Lee (JWL) Equation of State

The Jones–Wilkins–Lee (JWL) EOS [39] has been extensively used to model gaseous or solid explosives, and it has the form (27) with:

$$\Gamma(\rho) = \Gamma_0\,, \tag{29a}$$

$$\varepsilon_{\mathrm{r}}(\rho) = \frac{a}{r_1\rho_0}\mathrm{e}^{-r_1\frac{\rho_0}{\rho}} + \frac{b}{r_2\rho_0}\mathrm{e}^{-r_2\frac{\rho_0}{\rho}} - \varepsilon_0\,, \tag{29b}$$

$$p_{\mathrm{r}}(\rho) = a\,\mathrm{e}^{-r_1\frac{\rho_0}{\rho}} + b\mathrm{e}^{-r_2\frac{\rho_0}{\rho}}\,, \tag{29c}$$

where Γ_0, ρ_0, r_1, r_2, ε_0 are material-dependent parameters.

4.3. Noble–Abel Stiffened Gas (NASG) Equation of State

The Noble–Abel Stiffened Gas (NASG) Equation of State introduced in [37] combines the stiffened gas EOS [48] and the Noble–Abel EOS. It has the form:

$$p(\mathcal{E},\rho) = \frac{\gamma-1}{1-\rho b}(\mathcal{E} - \eta\rho) - \gamma\varpi\,, \tag{30a}$$

$$T(p,\rho) = \frac{(1-\rho b)(p+\varpi)}{\kappa_v\rho(\gamma-1)}. \tag{30b}$$

Here γ, ϖ, η, b, κ_v are material-dependent constant parameters. The coefficient b represents the covolume of the fluid and the choice $b = 0$ gives the classical stiffened gas equation of state. We can observe that the pressure law in (30a) has the form (27) with

$$\Gamma(\rho) = \tfrac{\gamma-1}{1-\rho\, b}\,, \quad \varepsilon_{\rm r} = \eta\,, \quad p_{\rm r} = -\gamma\varpi. \tag{31}$$

Let us also write the expression of the specific entropy s, the specific enthalpy h, and the chemical potential (equal for a pure constituent to its specific Gibbs free energy) $g = h - T\,s$:

$$s(p,T) = \kappa_v \log \frac{T^\gamma}{(p+\varpi)^{\gamma-1}} + \tilde\eta\,, \tag{32a}$$

$$h(T,p) = \kappa_p T + bp + \eta\,, \tag{32b}$$

$$g(p,T) = (\gamma\kappa_v - \tilde\eta)T - \kappa_v T \log \frac{T^\gamma}{(p+\varpi)^{\gamma-1}} + \eta + bp, \tag{32c}$$

where $\kappa_p = \gamma\kappa_v$ (specific heat capacity at constant pressure) and $\tilde\eta$ are constant parameters. Let us note that the speed of sound can be written:

$$c = \sqrt{\gamma \frac{p+\varpi}{\rho(1-\rho b)}}\,. \tag{33}$$

Finally, we can write the expressions for the derivatives in (16):

$$\phi = -\frac{\rho}{T}(1-\rho\, b) \qquad \text{and} \qquad \zeta = \frac{1}{T(\gamma-1)\kappa_v + b(p+\varpi)}(1-\rho\, b). \tag{34}$$

4.3.1. Saturation curves

For applications to two-phase flows with liquid-vapor transition, given the equation of state for each phase, the theoretical pressure-temperature saturation curve is determined by the equilibrium conditions $p_1 = p_2 = p$, $T_1 = T_2 = T$, $g_1(p,T) = g_2(p,T)$. Assuming here each phase governed by a NASG EOS, the equilibrium relations give the following equation:

$$A_s + \frac{B_s}{T} + C_s \log T + D_s \log(p+\varpi_1) - \log(p+\varpi_2) + \frac{p\,E_s}{T} = 0, \tag{35}$$

where

$$A_s = \frac{\kappa_{p1} - \kappa_{p2} - \tilde\eta_1 + \tilde\eta_2}{\kappa_{p2} - \kappa_{v2}},\ B_s = \frac{\eta_1 - \eta_2}{\kappa_{p2} - \kappa_{v2}},\ C_s = \frac{\kappa_{p2} - \kappa_{p1}}{\kappa_{p2} - \kappa_{v2}},\ D_s = \frac{\kappa_{p1} - \kappa_{v1}}{\kappa_{p2} - \kappa_{v2}},\ E_s = \frac{b_1 - b_2}{\kappa_{p2} - \kappa_{v2}}. \tag{36}$$

The constant parameters in the NASG equations of state of the two phases are determined so that the associated theoretical saturation curves match the experimental saturation curves for the considered material, at least in a certain temperature range, see [37]. The Tables 3-5 reported in Section 8 contain sets of parameters determined in [37] for water, Table 4 contains a slightly modified set of parameters for dodecane taken from [37].

5. Numerical method

We now consider the numerical solution of the six-equation model (1), which we rewrite here in compact vectorial form, denoting with $q \in \mathbb{R}^{5+d}$ the vector of the unknowns:

$$\partial_t q + \nabla \cdot f(q) + \sigma(q, \nabla q) = \psi_\mu(q) + \psi_\vartheta(q) + \psi_v(q)\,, \tag{37a}$$

$$q = \begin{bmatrix} \alpha_1 \\ \alpha_1\rho_1 \\ \alpha_2\rho_2 \\ \rho\vec{u} \\ \alpha_1 E_1 \\ \alpha_2 E_2 \end{bmatrix}, \quad f(q) = \begin{bmatrix} 0 \\ \alpha_1\rho_1\vec{u} \\ \alpha_2\rho_2\vec{u} \\ \rho\vec{u}\otimes\vec{u} + (\alpha_1 p_1 + \alpha_2 p_2)\,\mathbb{I} \\ \alpha_1\,(E_1 + p_1)\,\vec{u} \\ \alpha_2\,(E_2 + p_2)\,\vec{u} \end{bmatrix}, \quad \sigma\,(q, \nabla q) = \begin{bmatrix} \vec{u}\cdot\nabla\alpha_1 \\ 0 \\ 0 \\ 0 \\ \Sigma \\ -\Sigma \end{bmatrix}, \tag{37b}$$

$$\psi_\mu(q) = \begin{bmatrix} \mathcal{P} \\ 0 \\ 0 \\ 0 \\ -p_I\mathcal{P} \\ p_I\mathcal{P} \end{bmatrix}, \quad \psi_\vartheta(q) = \begin{bmatrix} 0 \\ 0 \\ 0 \\ 0 \\ \mathcal{Q} \\ -\mathcal{Q} \end{bmatrix}, \quad \psi_\nu(q) = \begin{bmatrix} 0 \\ \mathcal{M} \\ -\mathcal{M} \\ 0 \\ \left(g_I + \frac{|\vec{u}|^2}{2}\right)\mathcal{M} \\ -\left(g_I + \frac{|\vec{u}|^2}{2}\right)\mathcal{M} \end{bmatrix}, \tag{37c}$$

with $\Sigma(q, \nabla q)$ defined in (1g). Above we have put into evidence the conservative portion of the spatial derivative contributions in the system as $\nabla \cdot f(q)$, and we have indicated the non-conservative term as $\sigma(q, \nabla q)$. The source terms $\psi_\mu(q), \psi_\vartheta(q), \psi_\nu(q)$ contain mechanical, thermal and chemical relaxation terms, respectively, as expressed in (2).

To numerically solve this system we use a classical fractional step method, where we alternate between the solution of the homogeneous hyperbolic portion of the system via a wave-propagation finite volume scheme and the solution of a sequence of ordinary differential equations accounting for the relaxation source terms. Denoting with τ_μ, τ_ϑ, τ_ν the characteristic times for mechanical, thermal, and chemical relaxation, respectively, let us note that the underlying assumption here is $\tau_\mu \ll \tau_\vartheta \ll \tau_\nu$ (cf. for instance [31]). The algorithm consists of the following steps:

1. Solution of the homogeneous hyperbolic system

$$\partial_t q + \nabla \cdot f(q) + \sigma(q, \nabla q) = 0\,. \tag{38}$$

   In the following we will denote with the superscript 0 the quantities computed in this step.

2. Relaxation steps

   2(a) Instantaneous mechanical relaxation. We solve in the limit $\mu \to +\infty$ the system of ODEs

$$\partial_t q = \psi_\mu(q). \tag{39}$$

   This step drives instantaneously the flow to pressure equilibrium. We will denote with superscript $*$ the quantities computed in this step.

   2(b) Thermal relaxation. We solve

$$\partial_t q = \psi_\mu(q) + \psi_\vartheta(q), \tag{40}$$

   with $\mu \to +\infty$. This step drives the phases towards thermal equilibrium, while maintaining pressure equilibrium. We will denote with superscript $**$ the quantities computed in this step.

2(c) Chemical relaxation. We solve

$$\partial_t q = \psi_\mu(q) + \psi_\vartheta(q) + \psi_\nu(q), \tag{41}$$

with $\mu \to +\infty$. This step drives the phases towards full thermodynamical equilibrium, while maintaining pressure equilibrium. We will denote with superscript $\otimes$ the quantities computed in this step.

Let us first observe that the step 2(a) is always activated since we model flows in mechanical equilibrium. The steps 2(b) and 2(c) might be activated or not depending on the problem of interest, and, moreover, they might be activated only at selected locations, typically at interfaces, identified by $\min_k \alpha_k > \epsilon$, where ϵ is a given tolerance (e.g. 10^{-6}). If thermal and chemical relaxation are activated unconditionally then the numerical model approximates solutions to the pTg-relaxed model (24).

5.1. Mixture-energy-consistency

In the design of the fractional step method indicated above it is important to ensure *mixture-energy-consistency*, in the sense defined in [55]. Let us denote with superscript # the quantities computed in any of the relaxation steps of the above algorithm, $\# = *, **, \otimes$. Let us then denote with $E^{0,C}$ discrete values of the mixture total energy that come from a conservative approximation of the conservation law for E in (7). We say that the numerical scheme based on the fractional step algorithm above is mixture-energy-consistent if the following two properties are satisfied:

(i) Mixture total energy conservation consistency, i.e. conservation at the discrete level of the mixture total energy:

$$E^0 = E^{0,C}\,, \tag{42}$$

where $E^0 = (\alpha_1 E_1)^0 + (\alpha_2 E_2)^0$.

(ii) Relaxed pressure consistency, i.e. consistency of the values of the relaxed states with the mixture pressure law for pressure-equilibrium flows (12):

$$\mathcal{E}^0 = \alpha_1^\# \mathcal{E}_1(p^\#, \rho_1^\#) + \alpha_2^\# \mathcal{E}_2(p^\#, \rho_2^\#)\,, \tag{43}$$

where $\mathcal{E}^0 = E^0 - \frac{(\rho\vec{u})^0 \cdot (\rho\vec{u})^0}{2\rho^0}$.

6. Solution of the homogeneous system

To solve the hyperbolic homogeneous portion of (37) we employ the wave-propagation algorithms of [43, 42], which are a class of Godunov-type finite volume methods to approximate hyperbolic systems of partial differential equations. We shall consider here for simplicity the one-dimensional case in the x direction ($d = 1$), and we refer the reader to [43] for a comprehensive presentation of these numerical schemes. Hence we consider here the solution of the one dimensional system $\partial_t q + \partial_x f(q) + \sigma(q, \partial_x q) = 0$, $q \in \mathbb{R}^6$ (as obtained by setting $\vec{u} = u$ and $\nabla = \partial_x$ in (37)). We assume a grid with cells of uniform size Δx, and we denote with Q_i^n the approximate solution of the system at the ith cell and at time t^n, $i \in \mathbb{Z}$, $n \in \mathbb{N}$. The second-order wave propagation algorithm has the form

$$Q_i^{n+1} = Q_i^n - \frac{\Delta t}{\Delta x}(\mathcal{A}^+ \Delta Q_{i-1/2} + \mathcal{A}^- \Delta Q_{i+1/2}) - \frac{\Delta t}{\Delta x}(F^{\rm h}_{i+1/2} - F^{\rm h}_{i-1/2})\,. \tag{44}$$

Here $\mathcal{A}^{\mp}\Delta Q_{i+1/2}$ are the so-called fluctuations arising from Riemann problems at cell interfaces $(i+1/2)$ between adjacent cells i and $(i+1)$, and $F^{\mathrm{h}}_{i+1/2}$ are correction terms for (formal) second-order accuracy. To define the fluctuations, a Riemann solver (cf. [27, 75, 43]) must be provided. The solution structure defined by a Riemann solver can be expressed in general by a set of $\mathscr{M}$ waves $\mathcal{W}^l$ and corresponding speeds s^l, $\mathscr{M} \gtreqless 3N$. Once the Riemann solution structure $\{\mathcal{W}^l_{i+1/2}, s^l_{i+1/2}\}_{l=1,\dots,\mathscr{M}}$ arising at each cell edge $x_{i+1/2}$ is defined through a Riemann solver, the fluctuations $\mathcal{A}^{\mp}\Delta Q_{i+1/2}$ and the higher-order (second-order) correction fluxes $F^{\mathrm{h}}_{i+1/2}$ in (44) are computed as

$$\mathcal{A}^{\pm}\Delta Q_{i+1/2} = \sum_{l=1}^{\mathscr{M}} (s^l_{i+1/2})^{\pm} \mathcal{W}^l_{i+1/2}\,, \tag{45}$$

where we have used the notation $s^+ = \max(s, 0)$, $s^- = \min(s, 0)$, and

$$F^{\mathrm{h}}_{i+1/2} = \frac{1}{2} \sum_{l=1}^{\mathscr{M}} \left|s^l_{i+1/2}\right| \left(1 - \frac{\Delta t}{\Delta x} \left|s^l_{i+1/2}\right|\right) \mathcal{W}^{l\,\mathrm{h}}_{i+1/2}\,, \tag{46}$$

where $\mathcal{W}^{l\,\mathrm{h}}_{i+1/2}$ are a modified version of $\mathcal{W}^l_{i+1/2}$ obtained by applying to $\mathcal{W}^l_{i+1/2}$ a limiter function (cf. [43]). In the wave propagation scheme (44) we employ a simple HLLC-type Riemann solver, which we first presented in [55]. This solver is described in the Appendix C.

7. Relaxation processes

As indicated in Section 5, after solving the homogeneous system (38), we solve a sequence of systems of ordinary differential equations accounting for the relaxation source terms, namely the systems (39), (40), and (41). First of all, we observe that for any relaxation process we have

$$\partial_t \rho = 0\,, \tag{47a}$$

$$\partial_t (\rho \vec{u}) = 0\,, \tag{47b}$$

$$\partial_t E = 0\,. \tag{47c}$$

Therefore, the mixture density, velocity, total energy and internal energy remain constant during the transfer processes:

$$\rho = \text{const.}\,, \quad \vec{u} = \text{const.}\,, \quad E = \text{const.}\,, \quad \mathcal{E} = \text{const.}\,. \tag{48}$$

Moreover, if chemical relaxation is not activated, also the partial densities remain constant, since $\partial_t(\alpha_k\rho_k) = 0$, $k = 1, 2$:

$$\alpha_k\rho_k = \text{const.}\,. \tag{49}$$

To completely determine the relaxed states in the mechanical and thermal relaxation steps we need to determine two independent variables (here we choose as unknowns the volume fraction α_1 and the equilibrium pressure p). In the chemical relaxation step we have to determine instead three variables, since the partial densities vary. It is important to note that for consistency with the mixture equation of state for flows in mechanical equilibrium (12) the equilibrium pressure p determined in the all the relaxation steps should satisfy the energy relation (43).

7.1. Instantaneous relaxation processes

Before illustrating our new relaxation procedures, let us recall briefly the methods presented in our previous work [55] for instantaneous transfer processes. The idea is to use for each process the invariance relations (48), with also (49) for mechanical and thermal relaxation, and the corresponding equilibrium conditions to obtain an algebraic system for the unknown relaxed variables. Similar relaxation procedures for instantaneous processes can be also found for instance in [36, 34, 61]. We summarize here the equations to be used for each step of the algorithm in Section 5:

2(a) Instantaneous mechanical relaxation. We use the invariance relations (48) and (49) plus the mechanical equilibrium condition $p_1 = p_2 = p$. In this step we also need to integrate the phasic energy equations $\partial_t \mathcal{E}_k = (-1)^k p_\mathrm{I} \partial_t \alpha_1$, $k = 1, 2$ between the states 0 and $*$. To simplify the integration we make an assumption on the interface pressure p_I, which we define as a convex combination of the initial value p^0 and the equilibrium value p^*, $p_\mathrm{I} = \beta_p p^0 + (1-\beta_p) p^*, \beta_p \in [0, 1]$. In our previous work we set $\beta_p = \frac{1}{2}$ [55] or $\beta_p = 0$ [53]. We obtain an algebraic system of equations to be solved for two variables, for instance α_1^* and p^*. In the case of the stiffened gas EOS, the system can be reduced to the solution of a quadratic equation for the equilibrium pressure p^*.

2(b) Instantaneous mechanical and thermal relaxation. We use the invariance relations (48) and (49) plus the mechanical equilibrium condition $p_1 = p_2 = p$ and the thermal equilibrium condition $T_1 = T_2 = T$. We obtain an algebraic system of equations to be solved for two variables, for instance α_1^{**} and p^{**}. For the stiffened gas EOS, the system can be reduced to the solution of a quadratic equation for p^{**}.

2(c) Instantaneous mechanical, thermal and chemical relaxation. We use the invariance relations (48) plus the mechanical equilibrium condition $p_1 = p_2 = p$, the thermal equilibrium condition $T_1 = T_2 = T$, and the chemical equilibrium condition $g_1 = g_2$. We obtain an algebraic system to be solved for three variables, for instance $\alpha_1^\otimes$, $p^\otimes$, and $T^\otimes$. In general, an iterative method is necessary for the solution.

Let us remark that in all these relaxation procedures the energy relation (43) is ensured by construction, and the resulting algorithm is mixture-energy-consistent (we recall that (42) is guaranteed by the HLLC method).

7.2. Arbitrary-rate relaxation processes

As we have explained, we will always consider instantaneous mechanical relaxation processes, so we could adopt the mechanical relaxation procedure used in [55] and described above. Nonetheless, we will present below a new procedure for pressure relaxation based on an analytical semi-exact exponential solution, which is particularly advantageous for complex equations of state. It could be also potentially used for finite-rate pressure relaxation processes (e.g. [50]), which however are not of interest here.

Concerning heat and mass transfer, we wish to model here processes with arbitrary relaxation times, hence we wish to design algorithms capable of handling both instantaneous (stiff) processes and slow finite-rate ones. Let us consider the systems of ODEs in (40) and (41). We see that during thermal and chemical relaxation we need to guarantee pressure equilibrium, as represented by the presence in these systems of the pressure relaxation term ψ_μ with $\mu \to +\infty$.

In addition, during chemical relaxation, we need to account for the thermal relaxation effect, and in the limit of instantaneous thermal relaxation ($\vartheta \to +\infty$), we need to guarantee temperature equilibrium, as represented by the presence of the thermal source term ψ_ϑ in (41). Due to these constraints, for thermal and chemical relaxation it is not possible to use a simple fractional step method where each source term ψ_ϑ and ψ_ν in the six-equation model is integrated individually. On the other hand it appears very complicated to try to solve the ODEs with all the relaxation terms, which have very different characteristic time scales. Our idea consists in modifying the thermal and chemical relaxation terms ψ_ϑ and ψ_ν of the six-equation model to translate on them the effect of the instantaneous pressure relaxation term ψ_μ, and also to translate the effect of the thermal relaxation term ψ_ϑ on ψ_ν. Hence, we replace the system in (40) with a new system $\partial_t q = \tilde{\psi}_\vartheta$, where $\tilde{\psi}_\vartheta$ models thermal relaxation under pressure equilibrium, and we replace the system in (41) with a new system $\partial_t q = \tilde{\psi}_\nu$, where $\tilde{\psi}_\nu$ models chemical relaxation under pressure equilibrium and a thermal constraint, in particular thermal equilibrium. Our technique consists in employing in this approach the equations of the p-relaxed (9) and pT-relaxed (18) two-phase models. By using then some simplifying assumptions, analytical semi-exact exponential solutions are obtained to describe the relaxation processes.

Regarding computational efficiency, as we will detail in the following, in each relaxation step explicit expressions are employed to compute the independent variables of the relaxed states except for the equilibrium pressure, which in general is defined implicitly by the energy equation (12). This equation might require an iterative solution method. However, as previously noted, for equations of state that can be written in the form of the Mie–Grüneisen EOS (as in the numerical tests in Section 8) an explicit expression for p can be obtained (28), and no iterative method is required. The proposed new relaxation techniques are in general less computationally expensive with respect to the class of relaxation procedures for instantaneous transfers based on the solution of algebraic systems for the equilibrium states described in Section 7.1. Even in the simple case of the stiffened gas equation of state the chemical relaxation technique of the type described in Section 7.1 needs an iterative method to find the unknown equilibrium state, this being computationally more costly than the novel technique proposed here, which for the SG EOS employs explicit formulas only.

7.2.1. Mechanical relaxation

We propose here a new numerical procedure to model instantaneous mechanical relaxation. We start by writing the ordinary differential equations governing the relaxation process in terms of the volume fraction α_1 and the phasic pressures p_1 and p_2. Based on (1a) and (8) we have the equations:

$$\partial_t \alpha_1 = \mu(p_1 - p_2), \tag{50a}$$

$$\partial_t p_1 = \mu \frac{1}{\alpha_1} \left[\Gamma_1(\mathcal{E}_1 + p_1) + \chi_1 \rho_1\right](p_2 - p_1), \tag{50b}$$

$$\partial_t p_2 = -\mu \frac{1}{\alpha_2} \left[\Gamma_2(\mathcal{E}_2 + p_1) + \chi_2 \rho_2\right](p_2 - p_1), \tag{50c}$$

where $\mu > 0$ is considered a constant. The initial condition for the above system corresponds to the solution of the homogeneous system, denoted with superscript 0. Let us now introduce the quantities ξ_k^p, whose inverse values correspond to the terms multiplying $(p_2 - p_1)$ in the last two

equations of the system (50):

$$\frac{1}{\xi_k^p} = \frac{1}{\alpha_k}\left[\Gamma_k(\mathcal{E}_k + p_1) + \chi_k\rho_k\right] = \frac{1}{\alpha_k}\left[\Gamma_k(p_1 - p_k) + \rho_k c_k^2\right], \quad k = 1, 2\,. \tag{51}$$

We now introduce an approximation by assuming ξ_k^p constant in time, $\xi_k^p = \xi_k^{p0}$. Hence we consider the solution of

$$\partial_t p_1 = \mu \frac{1}{\xi_1^{p0}}(p_2 - p_1), \tag{52a}$$

$$\partial_t p_2 = -\mu \frac{1}{\xi_2^{p0}}(p_2 - p_1). \tag{52b}$$

From (52) we obtain the following ordinary differential equation for the pressure difference $\Delta p = p_2 - p_1$:

$$\partial_t \Delta p = -\mu\left(\frac{1}{\xi_1^{p0}} + \frac{1}{\xi_2^{p0}}\right)\Delta p, \tag{53}$$

which has the exact solution after a time interval Δt:

$$\Delta p^* = \Delta p^0 \mathrm{e}^{-K_p \Delta t}, \tag{54}$$

where

$$K_p = \mu\left(\frac{1}{\xi_1^{p0}} + \frac{1}{\xi_2^{p0}}\right). \tag{55}$$

We consider a process toward mechanical equilibrium, $K_p > 0$, as we expect from the pressure relaxation terms in the parent six-equation model where volume transfer occurs so that the phase with the lowest pressure is compressed, and the phase with the highest pressure is expanded if $\mu > 0$. We can now solve the partial differential equation for the volume fraction in (50a) by using the solution for Δp^* in (54). By integrating we find

$$\alpha_1^* = \alpha_1^0 - \frac{\Delta p^0}{\left(\frac{1}{\xi_1^{p0}} + \frac{1}{\xi_2^{p0}}\right)}(1 - \mathrm{e}^{-K_p \Delta t}). \tag{56}$$

In the limit of instantaneous pressure relaxation $\mu \to +\infty$ the above expression for α_1 gives the equilibrium value

$$\alpha_{1,\mu\to\infty}^* = \alpha_1^0 - \frac{\Delta p^0}{\left(\frac{1}{\xi_1^{p0}} + \frac{1}{\xi_2^{p0}}\right)}, \tag{57}$$

and the limit equilibrium pressure is:

$$p_{\mu\to\infty}^* = \frac{\xi_1^{p0} p_1^0 + \xi_2^{p0} p_2^0}{\xi_1^{p0} + \xi_2^{p0}}. \tag{58}$$

We might then use the two equilibrium quantities (57) and (58) to define the p-relaxed solution in the step (2a) of the algorithm. However, in contrast to the techniques for instantaneous relaxation

described in Section 7.1, in general the pair $\alpha^*_{1,\mu\to\infty}$ and $p^*_{\mu\to\infty}$ does not satisfy by construction the relation (43) (with # = $*$), due to the approximations in the ODEs solution. Hence here we define the updated volume fraction α^*_1 by using the exponential solution (57), but we update the equilibrium pressure by using the value p^* determined by the energy relation

$$\mathcal{E}^0 = \alpha^*_1 \mathcal{E}_1\left(p^*, \frac{(\alpha_1\rho_1)^0}{\alpha^*_1}\right) + \alpha^*_2 \mathcal{E}_2\left(p^*, \frac{(\alpha_2\rho_2)^0}{\alpha^*_2}\right). \tag{59}$$

The pressure relaxation procedure presented here is particularly convenient when complex equations of state are used. In fact the procedure used in [55] and recalled in Section 7.1 might lead to a complex algebraic system needing an iterative method for its solution. In Appendix D we also show that the relaxation procedure proposed here allows us to ensure velocity and pressure invariance at material interfaces at least when the stiffened gas equation of state is used. Let us finally observe that a similar mechanical relaxation procedure was proposed in [17]. However, in [17] the exponential solution for α_1 is assumed *a priori*, whereas here it is deduced from the model equations by assuming the quantities ξ^p_k constant in time during the relaxation process. Moreover in [17] the instantaneous equilibrium case was modeled by an exponential solution with very small relaxation time, whereas here we use the analytical limit (57).

7.2.2. Thermal relaxation

To describe the thermal relaxation process under the constraint of mechanical equilibrium $p_1 = p_2$ we consider here the ordinary differential equations with heat transfer source term corresponding to the reduced five-equation pressure equilibrium model (9). Specifically, we write the ODEs governing the thermal relaxation process for this model in terms of the volume fraction α_1, and the phasic temperatures T_1 and T_2. Based on (9a) and (15) we have the equations:

$$\partial_t \alpha_1 = \vartheta \frac{Z}{D}(T_2 - T_1), \tag{60a}$$

$$\partial_t T_1 = \vartheta \frac{1}{\phi_1 D}\left[-\frac{\rho_1}{\alpha_1} Z - \zeta_1(\Gamma_1\rho_2 c_2^2 - \Gamma_2\rho_1 c_1^2)\right](T_2 - T_1), \tag{60b}$$

$$\partial_t T_2 = \vartheta \frac{1}{\phi_2 D}\left[\frac{\rho_2}{\alpha_2} Z - \zeta_2(\Gamma_1\rho_2 c_2^2 - \Gamma_2\rho_1 c_1^2)\right](T_2 - T_1). \tag{60c}$$

where D is given in (10) and we have defined:

$$Z = \alpha_2\Gamma_1 + \alpha_1\Gamma_2\,. \tag{61}$$

The initial condition here corresponds to the pressure equilibrium solution coming from the mechanical relaxation step, denoted with the superscript $*$. Let us introduce the quantities ξ^T_k, whose inverse values correspond to the terms multiplying $(T_2 - T_1)$ in the last two equations of the above system:

$$\frac{1}{\xi^T_k} = -\frac{\frac{\rho_k}{\alpha_k} Z + (-1)^{k-1}\zeta_k(\Gamma_1\rho_2 c_2^2 - \Gamma_2\rho_1 c_1^2)}{\phi_k D}, \quad k = 1, 2\,. \tag{62}$$

Analogously to the pressure relaxation step we assume that the quantities ξ_k^T are constant in time, $\xi_k^T = \xi_k^{T*}$. Hence we consider the solution of

$$\partial_t T_1 = \vartheta \frac{1}{\xi_1^{T*}}(T_2 - T_1), \tag{63a}$$

$$\partial_t T_2 = -\vartheta \frac{1}{\xi_2^{T*}}(T_2 - T_1). \tag{63b}$$

We also consider that $\vartheta > 0$ is a constant. If ϑ is a given function of some variables instead of a constant parameter, then we fix ϑ to its value at the state $*$. From (63) we obtain the following ordinary differential equation for the temperature difference $\Delta T = T_2 - T_1$:

$$\partial_t \Delta T = -\vartheta \left(\frac{1}{\xi_1^{T*}} + \frac{1}{\xi_2^{T*}} \right) \Delta T, \tag{64}$$

which has the following exact solution after a time step Δt:

$$\Delta T^{**} = \Delta T^* \mathrm{e}^{-K_T \Delta t}, \tag{65}$$

where

$$K_T = \vartheta \left(\frac{1}{\xi_1^{T*}} + \frac{1}{\xi_2^{T*}} \right). \tag{66}$$

We consider a process toward thermal equilibrium, $K_T > 0$, as we expect from the temperature relaxation terms in the parent six-equation model where heat transfer occurs from the hotter to the colder phase if $\vartheta > 0$. We now need to solve the partial differential equation for the volume fraction in (60a). Assuming that Z/D is constant and by using the solution for ΔT^{**} in (65) we obtain

$$\alpha_1^{**} = \alpha_1^* + \left(\frac{Z}{D} \right)^* \frac{\Delta T^*}{\left(\frac{1}{\xi_1^{T*}} + \frac{1}{\xi_2^{T*}} \right)} (1 - \mathrm{e}^{-K_T \Delta t}). \tag{67}$$

In the limit of instantaneous temperature relaxation $\vartheta \to +\infty$ the above expression for α_1 gives the equilibrium value

$$\alpha_{1,\,\vartheta\to\infty} = \alpha_1^* + \left(\frac{Z}{D} \right)^* \frac{\Delta T^*}{\left(\frac{1}{\xi_1^{T*}} + \frac{1}{\xi_2^{T*}} \right)}, \tag{68}$$

and the equilibrium temperature is:

$$T_{\vartheta\to\infty} = \frac{\xi_1^{T*} T_1^* + \xi_2^{T*} T_2^*}{\xi_1^{T*} + \xi_2^{T*}}. \tag{69}$$

To update the solution at the step (2b) of the algorithm we use the relaxed value α_1^{**} in (67) (or in (68) in case of instantaneous relaxation), and the pressure value p^{**} determined by the energy relation

$$\mathcal{E}^0 = \alpha_1^{**} \mathcal{E}_1 \left(p^{**}, \frac{(\alpha_1 \rho_1)^0}{\alpha_1^{**}} \right) + \alpha_2^{**} \mathcal{E}_2 \left(p^{**}, \frac{(\alpha_2 \rho_2)^0}{\alpha_2^{**}} \right) \tag{70}$$

in order to ensure mixture-energy-consistency.

7.2.3. Chemical relaxation

The chemical relaxation process occurs under mechanical equilibrium and it is coupled to a thermal relaxation process which is assumed much faster than the chemical relaxation one. Hence, it is often reasonable to consider a chemical relaxation process occurring under both mechanical and thermal equilibrium, and here we consider this case. To describe this process we use then the ordinary differential equations with mass transfer source term corresponding to the reduced four-equation pressure and temperature equilibrium model (18). Specifically, we wish to write the ODEs governing the chemical relaxation process for this model in terms of the volume fraction α_1, the partial density $\alpha_1\rho_1$, and the phasic chemical potentials g_1 and g_2. First, let us note that the ordinary differential equations for α_1 and $\alpha_1\rho_1$ are given by $\partial_t\alpha_1 = \mathcal{S}_\alpha\mathcal{M}$ and $\partial_t(\alpha_1\rho_1) = \mathcal{M}$, respectively, based on (23) and (18). We can then write the ordinary differential equations governing the phasic chemical potentials g_k, by writing $\partial_t g_k = \frac{1}{\rho_k}\partial_t p_k - s_k\partial_t T_k$ and by using the equations $\partial_t T = \mathcal{S}_T\mathcal{M}$ and $\partial_t p = \mathcal{S}_p$ obtained from (23). We obtain the system:

$$\partial_t\alpha_1 = \nu\mathcal{S}_\alpha(g_2 - g_1), \tag{71a}$$

$$\partial_t g_1 = \nu\left(\frac{\mathcal{S}_p}{\rho_1} - s_1\mathcal{S}_T\right)(g_2 - g_1), \tag{71b}$$

$$\partial_t g_2 = \nu\left(\frac{\mathcal{S}_p}{\rho_2} - s_2\mathcal{S}_T\right)(g_2 - g_1), \tag{71c}$$

$$\partial_t(\alpha_1\rho_1) = \nu(g_2 - g_1). \tag{71d}$$

Note that the interface chemical potential g_I does not appear anymore in the equations (cf. also the pT-relaxed model), hence a definition for this quantity is not needed. The initial condition for (71) corresponds to the solution coming from the thermal relaxation step, denoted with superscript $**$. Let us introduce the quantities ξ_k^g, whose inverse values correspond to the terms multiplying $(g_2 - g_1)$ in the two equations for g_k of the above system:

$$\frac{1}{\xi_k^g} = \frac{(-1)^{k-1}}{\rho_k}\mathcal{S}_p - s_k\mathcal{S}_T\,, \quad k = 1, 2\,. \tag{72}$$

Analogously to the pressure and temperature relaxation step we assume that the quantities ξ_k^g are constant in time, $\xi_k^g = \xi_k^{g**}$. Hence we consider the solution of

$$\partial_t g_1 = \nu\frac{1}{\xi_1^{g**}}(g_2 - g_1), \tag{73a}$$

$$\partial_t g_2 = -\nu\frac{1}{\xi_2^{g**}}(g_2 - g_1). \tag{73b}$$

We also consider that $\nu > 0$ is a constant. If ν is a given function of some variables instead of a constant parameter, then we fix ν to its value at the state $**$. From (73) we obtain the following ordinary differential equation for the chemical potential difference $\Delta g = g_2 - g_1$:

$$\partial_t\Delta g = -\nu\left(\frac{1}{\xi_1^{g**}} + \frac{1}{\xi_2^{g**}}\right)\Delta g, \tag{74}$$

which has the exact solution after a time interval Δt:

$$\Delta g^{\otimes} = \Delta g^{**} \mathrm{e}^{-K_g \Delta t}, \tag{75}$$

where

$$K_g = \nu \left(\frac{1}{\xi_1^{g**}} + \frac{1}{\xi_2^{g**}} \right). \tag{76}$$

We consider a process toward chemical equilibrium, $K_g > 0$, as we expect from the chemical potential relaxation terms in the parent six-equation model where mass transfer occurs from the phase with the highest chemical potential toward the phase with the lowest if $\nu > 0$. We now need to solve the partial differential equation for the volume fraction in (71a) and the partial density $\alpha_1\rho_1$ in (71d). By using the solution for $\Delta g^{\otimes}$ in (75) we immediately obtain

$$(\alpha_1\rho_1)^{\otimes} = (\alpha_1\rho_1)^{**} + \frac{\Delta g^{**}}{\left(\frac{1}{\xi_1^{g**}} + \frac{1}{\xi_2^{g**}} \right)} (1 - \mathrm{e}^{-K_g \Delta t}). \tag{77}$$

Assuming now that $\mathcal{S}_\alpha$ is constant, for the volume fraction we get

$$\alpha_1^{\otimes} = \alpha_1^{**} + \mathcal{S}_\alpha^{**} \frac{\Delta g^{**}}{\left(\frac{1}{\xi_1^{g**}} + \frac{1}{\xi_2^{g**}} \right)} (1 - \mathrm{e}^{-K_g \Delta t}). \tag{78}$$

In the limit of instantaneous chemical relaxation $\nu \to +\infty$ the above expressions for $\alpha_1\rho_1$ and α_1 give the equilibrium values

$$(\alpha_1\rho_1)_{\nu\to\infty} = (\alpha_1\rho_1)^{**} + \frac{\Delta g^{*}}{\left(\frac{1}{\xi_1^{g**}} + \frac{1}{\xi_2^{g**}} \right)}, \tag{79}$$

$$\alpha_{1,\,\nu\to\infty} = \alpha_1^{*} + \mathcal{S}_\alpha^{**} \frac{\Delta g^{*}}{\left(\frac{1}{\xi_1^{g**}} + \frac{1}{\xi_2^{g**}} \right)}, \tag{80}$$

and the equilibrium chemical potential is:

$$g_{\nu\to\infty} = \frac{\xi_1^{g**} g_1^{**} + \xi_2^{g**} g_2^{**}}{\xi_1^{g**} + \xi_2^{g**}}. \tag{81}$$

To update the solution at the step (2c) of the algorithm we use the relaxed values $(\alpha_1\rho_1)^{\otimes}$ and $\alpha_1^{\otimes}$ in (77) and (78) (or in (79) and (80) in case of instantaneous relaxation), and the pressure value $p^{\otimes}$ is determined by the energy relation

$$\mathcal{E}^0 = \alpha_1^{\otimes} \mathcal{E}_1 \left(p^{\otimes}, \frac{(\alpha_1\rho_1)^{\otimes}}{\alpha_1^{\otimes}} \right) + \alpha_2^{\otimes} \mathcal{E}_2 \left(p^{\otimes}, \frac{(\alpha_2\rho_2)^{\otimes}}{\alpha_2^{\otimes}} \right) \tag{82}$$

in order to ensure mixture-energy-consistency. Let us remark that although the equations (71) above have been obtained by assuming temperature equilibrium $T_2 = T_1 = T$ (in addition to pressure equilibrium), they hold more generally in the hypothesis of a chemical relaxation process occurring at constant temperature difference $T_2 - T_1 = \Delta T$, since in this case $\partial T_1 = \partial T_2$ and the derivation of (23) in Appendix B can be easily extended to the case in which the variables associated to the phase k are functions of p and T_k with the constraint $T_2 = T_1 + \Delta T$, ΔT = constant. Hence the procedure described in this Section could be also employed to model chemical relaxation processes with thermal disequilibrium, provided consistent relaxation times are chosen, since thermal relaxation is physically faster than chemical relaxation.

Complete evaporation or condensation

It is physically possible that the mass transfer process leads to complete evaporation or complete condensation, thus to the disappearance of one phase. In such a case the computation via (78) (or (80)) produces a value $\alpha_1^{\otimes} \notin (0,1)$. To handle this case numerically we proceed as follows. First, let us recall that in our numerical model both phases must always be present, therefore we model a pure phase k as a mixture with a volume fraction $\alpha_k = 1 - \epsilon_\alpha$, where $0 < \epsilon_\alpha \ll 1$ (e.g. $\epsilon_\alpha = 10^{-8}$). If in the numerical computation we find $\alpha_1^{\otimes} \notin (0,1)$ we consider that one phase vanishes hence we set $\alpha_1^{\otimes} = \bar{\alpha}_1$ where $\bar{\alpha}_1 = \epsilon_\alpha$ if $s_2^{**} > s_1^{**}$ (vanishing of phase 1), or $\bar{\alpha}_1 = 1 - \epsilon_\alpha$ if $s_1^{**} > s_2^{**}$ (vanishing of phase 2). Then we determine the value of the relaxation parameter K_g that gives the value $\bar{\alpha}_1$ through the formula (78). We find:

$$\bar{K}g = -\frac{1}{\Delta t} \log\left(1 - \frac{\bar{\alpha}_1 - \alpha_1^{**}}{\mathcal{S}_\alpha^{**} \frac{\Delta g^{**}}{\left(\frac{1}{\xi_1^{g**}} + \frac{1}{\xi_2^{g**}} \right)}} \right). \tag{83}$$

Finally we set $(\alpha_1\rho_1)^{\otimes}$ by using the formula (77) with $K_g = \bar{K}_g$. Let us remark that if an unphysical value of α_1 is computed in the pressure and temperature relaxation procedures previously presented, it suffices to set $\alpha_1 = \bar{\alpha}_1$.

8. Numerical experiments

We present in this section several numerical experiments in one and two dimensions. The algorithm has been implemented by using the basic routines of the CLAWPACK software [41]. All the computations have been performed with the second-order wave propagation scheme with the minmod limiter. In some one-dimensional Riemann problems we plot the exact solution for the p-relaxed model (9) (see [58]) and the pT-relaxed model (18). These exact solutions have been computed by extending to the models (9) and (18) the methodology detailed in [30, 29] for the compressible single-phase Euler equations with general equation of state.

8.1. Numerical tests with only mechanical relaxation

We begin by presenting some numerical experiments where we activate only instantaneous mechanical relaxation. The aim in particular is to show the good performance of the numerical model when complex equations of state are employed in problems with strong shocks and interfaces.

8.1.1. Detonation gas-water shock tube

We consider a two-fluid one-dimensional shock tube problem over the domain $[-10, 10]$ m. There is an initial discontinuity at $x = 0$ that separates a left region filled with detonation gases with density $\rho_{\text{gas}} = 2000\,\text{kg} \cdot \text{m}^{-3}$ and pressure $p_{\text{gas}} = 4.6406 \cdot 10^{10}$ Pa, and a right region filled with liquid water with density $\rho_{\text{liq}} = 1044\,\text{kg} \cdot \text{m}^{-3}$ and pressure $p_{\text{liq}} = 10^5$ Pa. Detonation gases are modeled by the JWL equation of state with the parameters in Table 2 (taken from [60]), and the liquid water is modeled by the NASG equation of state with the parameters in Table 3. In each region we consider a nearly pure fluid with volume fraction $1 - 10^{-8}$. The initial velocity is $u = 0$. We compute the solution with 500 grid cells and CFL number = 0.4. In Figure 1 we show results at $t = 0.9$ ms for the density, velocity, pressure, and gas volume fraction, together

with the exact solution for this problem. We observe the agreement with the exact solution and in particular the ability of the method to preserve velocity and pressure invariance across and around the material interface.

Table 2: Material properties for the JWL equation of state modeling explosive.

Parameter	Value (Explosive)	Units
ρ_0	1840	[kg/m^3]
Γ_0	0.25	
a	854.5×10^9	[Pa]
b	20.5×10^9	[Pa]
r_1	4.6	
r_2	1.35	
ε_0	0	[J/kg]

Table 3: Parameters for the NASG EOS for liquid and vapor water in the temperature range 300-500 K

phase	γ	ϖ [Pa]	η [J/kg]	$\tilde{\eta}$ [J/(Kg $\cdot$ K)]	κ_v [J/(Kg $\cdot$ K)]	b [m^3/kg]
liquid	1.187	7028×10^5	-1177788	0	3610	6.61×10^{-4}
vapor	1.467	0	2077616	14317	955	0

8.1.2. Underwater explosion close to a rigid wall

We now perform a two-dimensional experiment. In this test we simulate a cylindrical underwater explosion (UNDEX) in proximity to a rigid upper surface. We consider a variant of the test presented in [78], where the authors use a single-fluid cavitation model with a barotropic equation of state for the liquid (Tait's EOS) and an ideal gas equation of state for the gas. This test was presented by the same authors also in [79]. We consider an initial bubble of highly pressurized gas (combustion products) surrounded by liquid water and located near an upper flat wall. Combustion gases are modeled by the JWL equation of state with the parameters in Table 2, while liquid water is modeled by the NASG EOS with the parameters in Table 3. The considered domain is $[-1.35, 1.35] \times [-1.5, 0]$ m^2, with the wall at $y = 0$ m. The bubble initially is located at $(x_b, y_b) = (0, -0.32)$ m, and it has radius $r_b = 0.05$ m. Inside the bubble we set initially a pressure $p = 4.6406 \cdot 10^{10}$ Pa, a gas density $\rho_{gas} = 2000\,\mathrm{kg/m^3}$, and a gas volume fraction $\alpha_{gas} = 1 - 10^{-6}$. Outside the bubble we set a pressure $p = 10^5$ Pa, a liquid density $\rho_{liq} = 1044\,\mathrm{kg/m^3}$ and a liquid volume fraction $\alpha_{liq} = 1 - 10^{-6}$. Note that the states inside and outside the bubble correspond to the left and right states of the one-dimensional gas-water shock tube in the previous Section. This explosion problem is characterized by a complex pattern of shocks and rarefaction waves [13, 78, 79], which the proposed computational model is able to predict qualitatively. We use 721×400 grid cells with CFL number = 0.4. We show in Figure 2 plots of the pressure field at six different times (the x-interval of the plots is $[-1, 1]$ m, smaller than the computational one to better observe the relevant features of the results). In Figure 3 moreover we plot the time history of the pressure recorded at the point $(0, 0)$ at the center of the flat upper surface until time $t = 0.4$ ms. At $t = 0.03$ ms (upper right plot in Fig. 2) we can observe the circular shock created by the explosion. In the subsequent plots the shock has reflected from the wall. The shock reflection gives rise to rarefactions that cause a strong pressure decrease in the zone close to the wall, followed later by a moderate recompression

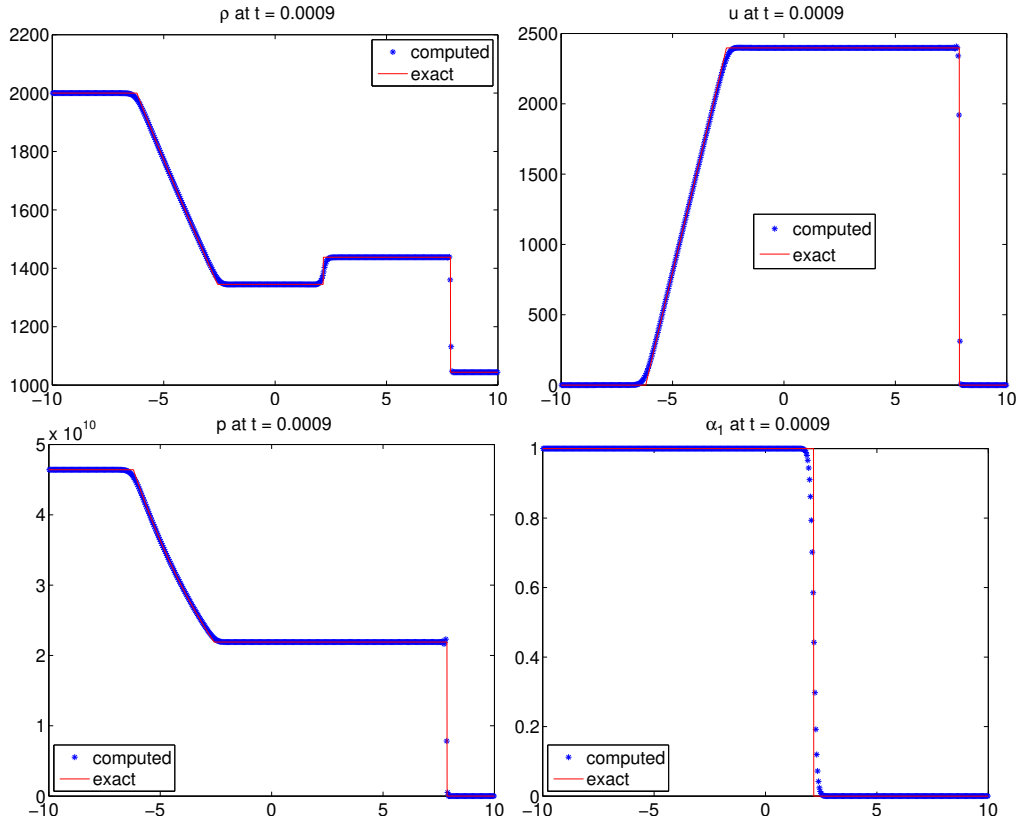

Figure 1: Detonation gas-water shock tube problem. Computed results for the density ρ, velocity u, pressure p, and gas volume fraction α_1 at time $t = 0.9$ ms (blue marks $*$), compared with the exact solution (solid red line).

and then by another expansion. The minimum pressure at the center of the wall is reached at around $t = 0.21$ ms (corresponding to the lower left plot in Fig. 2), the maximum pressure in the following recompression is reached at about $t = 0.3$ ms (lower right plot in Fig. 2). Let us note that with the chosen setup the expansion regions near the wall do not reach very low pressure values as in the case of cavitation occurrence, see in this respect for instance the different cases in [79] related to the chosen geometrical configuration.

8.2. Numerical tests with thermo-chemical relaxation

We now present several numerical experiments where we activate thermal and chemical relaxation, simulating both instantaneous and finite-rate transfer processes. Concerning non-instantaneous transfers we report primarily tests with finite-rate mass transfer under thermal equilibrium, which is our principal interest.

8.2.1. Water two-phase cavitation tube

We consider a one-dimensional water cavitation tube problem, which is a variant of a numerical test taken from [65] that we performed in [55] with the stiffened gas equation of state and instantaneous relaxation processes. Initially we have a tube over the interval $[0, 1]$ m filled

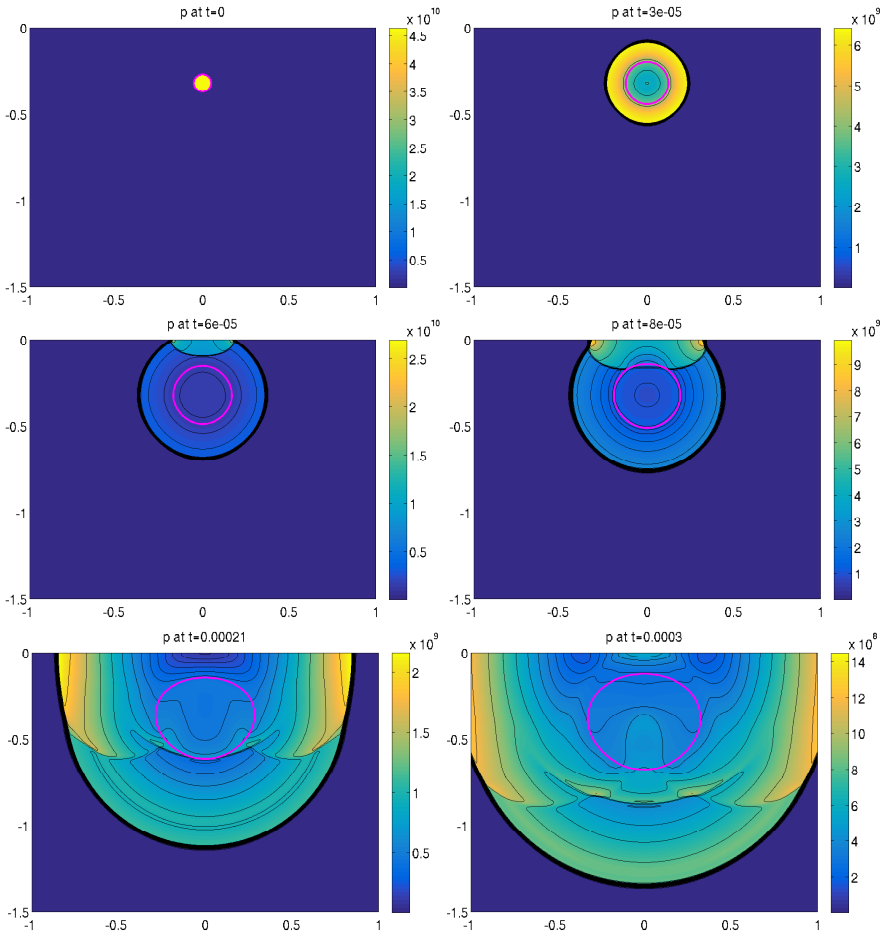

Figure 2: Underwater explosion near a rigid upper flat surface. Computed pressure field at times t = 0, 0.03, 0.06, 0.08, 0.21, 0.3 ms. The thick solid line (magenta color) indicates the water/bubble interface.

with liquid water with a uniformly distributed small amount of vapor, with a volume fraction $\alpha_{\text{vap}} = 10^{-2}$ in the whole domain. Initially the pressure is $p = 10^5$ Pa and the temperature $T = T_1 = T_2 = 353$ K, which is less than the saturation temperature $T_{\text{sat}}(p) = 372.3$ K. Note that initially the phases are in thermal equilibrium but not in chemical equilibrium. A velocity discontinuity is set at $x = 0.5$ m at initial time, with $u = -2$ m/s on the left and $u = 2$ m/s on the right. We use here the NASG equation of state for the liquid water and water vapor phases, with the parameters in Table 3. We perform computations with five different levels of relaxation by using the techniques detailed in Section 7.2: only instantaneous mechanical relaxation (case denoted as p-relax in the plots), instantaneous mechanical relaxation and finite-rate thermal relaxation with $\vartheta = 2000$ Pa/(s · K) (pT(f)), instantaneous mechanical and thermal relaxation (pT), instantaneous mechanical and thermal relaxation and finite-rate chemical relaxation with $\nu = 10^{-4}$ Pa · kg^2/(s · J^2) (pTg(f)), and full thermodynamic relaxation (pTg). Phase transition is hence activated only in the two last cases. Let us remark that in this test (following [65])

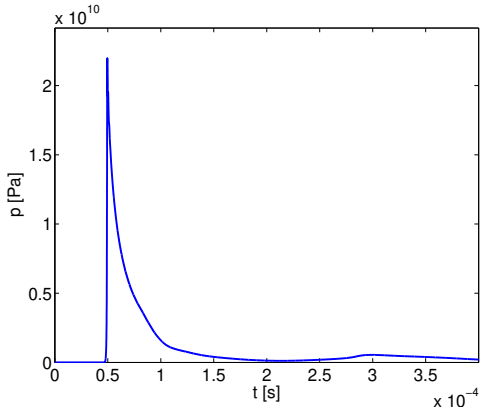

Figure 3: Underwater explosion near a rigid upper flat surface. Time history of the pressure at the point $(0, 0)$ at the middle of the upper surface.

chemical relaxation is activated when the equilibrium temperature is greater than the saturation temperature, $T > T_{\text{sat}}(p)$ (this happens in the middle region of the tube as one can see from the plot of the chemical potentials in Figure 5). For this reason, and because of the setup with initial chemical potential disequilibrium, we note that the solution computed here with activation of full thermodynamic relaxation (and indicated pTg) does not correspond to a solution of the HEM model (24). We use 5000 grid cells and we set the CFL number = 0.5. Results for the pressure, velocity, vapor volume fraction and vapor mass fraction at time $t = 0.003$ s are displayed in Figure 4. In all the cases the solution involves two rarefactions going in opposite directions that cause a decrease of the pressure in the middle of the tube, and correspondingly an increase of the vapor volume fraction. Let us note that if mass transfer is not activated then the vapor mass fraction remains constant, and the cavitation process is only mechanical. In contrast, if mass transfer is activated then the solution involves also two evaporation waves. In this case the vapor mass fraction increases in the middle of the tube, and moreover here the pressure is driven to its saturation value, whereas without mass transfer the pressure continues to decrease in the center of the tube. In Figure 5 we show the equilibrium temperature and the chemical potentials for the three test cases with instantaneous pressure and temperature equilibrium (pT, pTg(f), pTg), with or without mass transfer. Computed liquid and vapor temperatures are found to be overlapped, this proving the ability to numerically impose thermal equilibrium. By observing the plot of the liquid and vapor chemical potentials we notice the region of chemical potential equilibrium in the middle of the tube for the pTg-relaxation case, corresponding to the region of activation of chemical relaxation under the evaporation condition $T > T_{\text{sat}}$. For the case with finite rate mass transfer (pT(f)-relaxation) we notice that liquid and vapor chemical potentials are being driven to equilibrium and their difference is correctly reduced with respect to the case with no mass transfer (pT-relaxation). In Figures 4, 5 we also plot the exact solution for this problem of the five-equation pressure equilibrium model (9) and of the four-equation pressure and temperature equilibrium model (18). We observe good agreement of the results computed with activation of instantaneous mechanical relaxation with the exact solution of the five-equation p-relaxed model, and of the results computed with activation of instantaneous mechanical and thermal relaxation with the exact solution of the four-equation pT-relaxed model. This shows

the capability of the numerical model to approximate solutions of the limit equilibrium models in the limit on instantaneous relaxation processes. Let us also observe that the different speeds of the leading edges of the rarefactions for different levels of activation of relaxation processes is consistent with the subcharacteristic condition in (26) $c_{pT} \leq c_p$. Note that also in the tests with phase transition in correspondence of these leading edges the sound speed is the pressure and temperature equilibrium sound speed c_{pT} (19) (and not c_{pTg} (25), which would be much smaller), since in these zones chemical relaxation is not activated since $T < T_{\text{sat}}$.

8.2.2. Dodecane liquid-vapor shock tube

We consider here a dodecane liquid-vapor shock tube problem also proposed in [65], which we solved in [55] with the stiffened gas equation of state. This test involves a unit length shock tube with an initial discontinuity located at $x = 0.75$ m that separates a left region filled with liquid dodecane and a right region filled with vapor dodecane. As in [65], for numerical reasons each fluid region contains a small amount of the phase that fills the region on the other side of the discontinuity ($\alpha = 10^{-8}$). The initial condition consists of two constant states on the two sides of the discontinuity with pressure $p = 10^8$ Pa on the left and $p = 10^5$ Pa on the right. The initial velocity is $u = 0$, and the initial values of the vapor and liquid densities are $\rho_{\text{vap}} = 2 \text{ kg} \cdot \text{m}^3$ and $\rho_{\text{liq}} = 500 \text{ kg} \cdot \text{m}^3$, respectively. The liquid and vapor phases of dodecane are modeled by the NASG equation of state with the parameters given in Table 4. We use 2000 grid cells and we set CFL = 0.5. Figure 6 shows numerical results at time $t = 473$ μs obtained by employing our numerical model with and without heat and mass transfer effects. More precisely, we plot results for two different levels of relaxation: instantaneous mechanical relaxation (p-relax in the plots), and instantaneous full thermodynamical relaxation (pTg-relax). Let us note that for the latter case thermo-chemical relaxation is activated only at interfaces, defined by $\min(\alpha_{\text{vap}}, \alpha_{\text{liq}}) > \epsilon$, $\epsilon = 10^{-4}$, and chemical relaxation is activated under the condition $T > T_{\text{sat}}$. We can observe for both cases with and without phase transition that the solution consists of a leftward going rarefaction wave, a rightward going contact discontinuity, and a shock wave. Moreover, when thermal and chemical effects are activated liquid-vapor phase change occurs, generating an additional evaporation wave between the rarefaction wave and the contact discontinuity. This evaporation front produces a liquid-vapor saturation region at higher speed. Note that the left-going rarefaction occurs in a region of almost pure liquid (α_{vap} nearly zero) and, as noted above, only mechanical relaxation is activated in this zone for any case (p- and pTg-relaxation), hence the phases have different temperatures. Let us also remark that in this left zone the vapor temperature has no physical meaning, and since the value that it reaches is unphysically high, of the order of 10^6 K, we have plotted the temperatures in Figure 6 only over the physical range with a maximum temperature value of 1200 K, to be able to observe the relevant liquid and vapor temperature curves. For the pTg-relaxation case the liquid-vapor transition leads to complete evaporation (handled with the technique illustrated in Section 7.2.3, see (83)), and on the right end of the interval there is a region of nearly pure vapor. Again, in this region of nearly pure vapor (α_{liq} nearly zero) only mechanical relaxation is activated. We can notice from the temperatures plot in Figure 6 the small liquid-vapor mixture zone where thermo-chemical relaxation is activated and where thermal and chemical equilibrium is imposed. This corresponds to the zone where the vapor and liquid temperature curves of the pTg-relaxed computation overlap around $\approx x = 0.83$ m (solid and dashed blue lines). In the plots we also display the exact solution of the five-equation pressure equilibrium model for this problem, and we observe good agreement with this solution of our results with mechanical relaxation only.

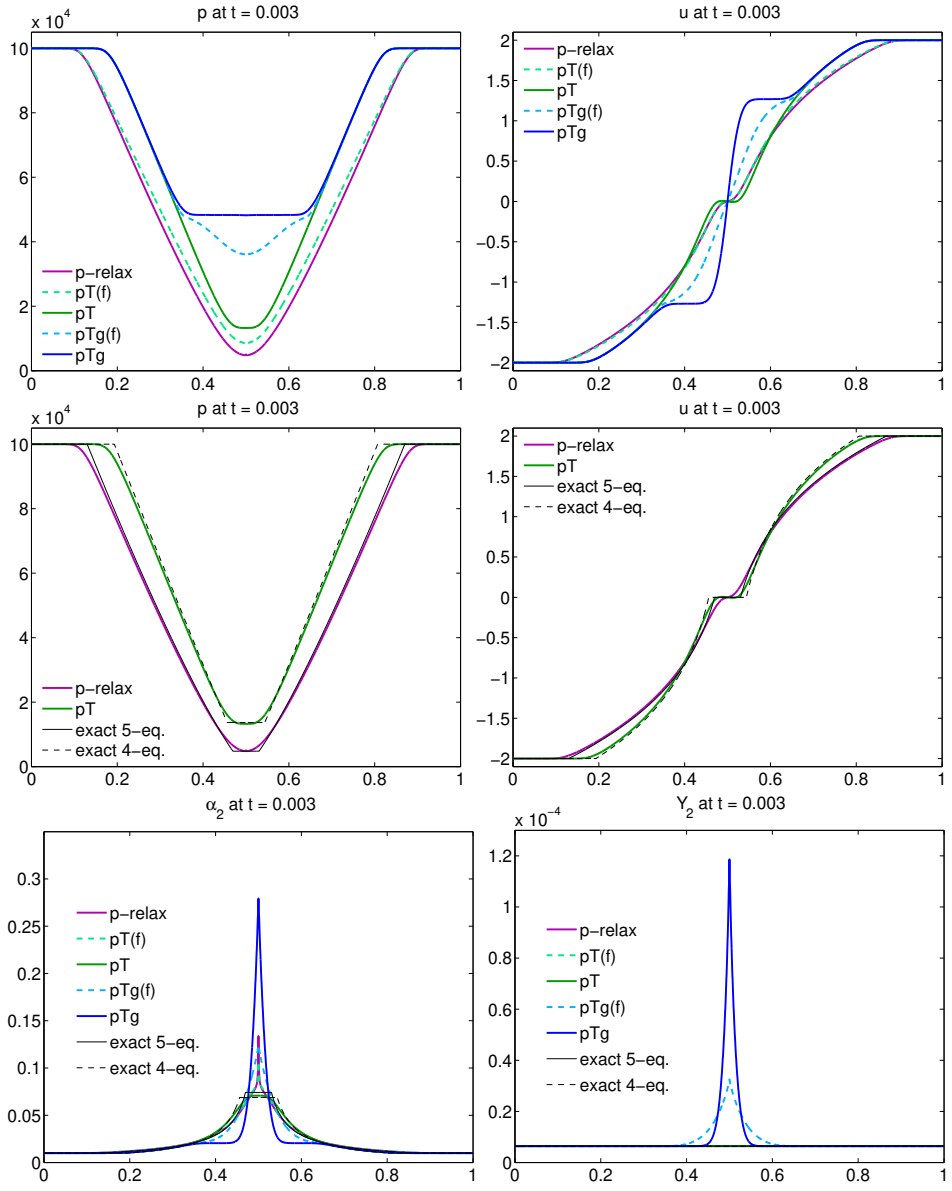

Figure 4: Water cavitation tube test, results at $t = 0.003$ s. Pressure p, velocity u, vapor volume fraction α_2, vapor mass fraction Y_2 for five levels of relaxation. p-relax (violet solid line): instantaneous mechanical relaxation; pT(f) (dashed light green line): instantaneous mechanical relaxation and finite-rate thermal relaxation; pT (solid dark green line): instantaneous mechanical and thermal relaxation; pTg(f) (dashed light blue line): instantaneous mechanical and thermal relaxation and finite-rate chemical relaxation; pTg (solid dark blue line): instantaneous mechanical, thermal, and chemical relaxation. The exact solution of the p-relaxed model (solid black line) and of the pT-relaxed model (dashed black line) is also plotted. For better clarity the comparison with these exact solutions for p and u has been displayed separately in the second row of plots.

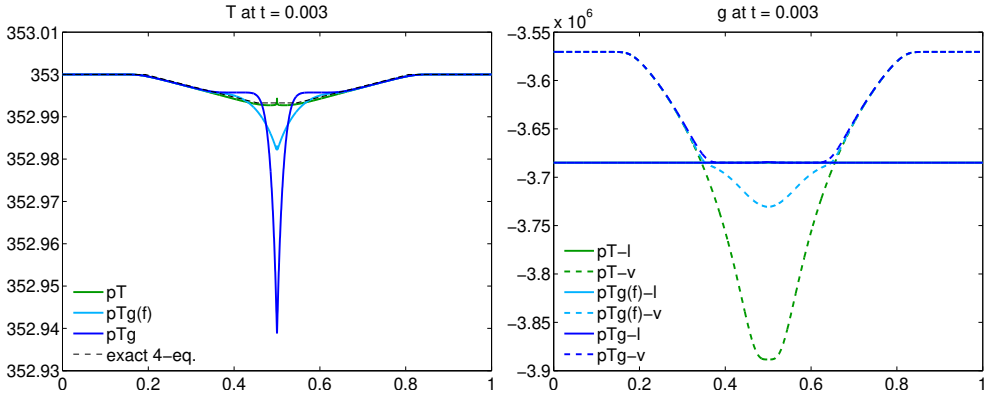

Figure 5: Water cavitation tube test, results at $t = 0.003$ s. Equilibrium temperature T and chemical potentials g_k for the test cases with temperature equilibrium (results for the liquid and vapor temperature are overlapped so we plot a single line for T). pT (dark green line): instantaneous mechanical and thermal relaxation; pTg(f) (light blue line): instantaneous mechanical and thermal relaxation and finite-rate chemical relaxation; pTg (dark blue line): instantaneous mechanical, thermal, and chemical relaxation. In the plot of the chemical potentials g_k the solid line indicates the liquid (l) and the dashed line the vapor (v). Results for the liquid and vapor chemical potential for the pTg case overlap in the central region. The exact temperature solution of the four-equation pT-relaxed model (dashed black line) is also plotted.

Table 4: Parameters for the NASG EOS for liquid and vapor dodecane in the temperature range 400-600 K

phase	γ	ϖ [Pa]	η [J/kg]	$\tilde{\eta}$ [J/(Kg · K)]	κ_v [J/(Kg · K)]	b [m^3/kg]
liquid	1.206	1681×10^5	−996054	0	2532	7.51×10^{-4}
vapor	1.021	0	−384592	−4301	2274	0

8.2.3. Simões-Moreira & Shepherd dodecane evaporation tests

For validation purposes, following [65], we now perform a set of dodecane shock tube tests similar to the numerical test of the previous section to compare computed results for the velocities of the evaporation front with the experimental results reported by Simões-Moreira and Shepherd [72]. These authors performed tests where liquid dodecane in a tube was suddenly discharged into a low-pressure chamber by breaking a diaphragm, this depressurizing the liquid and initiating evaporation. The initial reservoir pressure was about 1 mbar, and tests were carried out for eight values of the test temperature T_{test} from 180°C to 300°C. We perform numerical tests for the same set of temperatures. As done by others authors in the literature [65, 80, 59] we consider here instantaneous mass transfer and we model liquid and vapor dodecane by a stiffened gas equation of state, with the parameters for dodecane used in [55], which allow a good matching with the experimental saturation curve in the considered temperature range. The temperature value T_{test} is initially set everywhere in the tube. In the low-pressure chamber we set $p = 1$ mbar as in the laboratory experiments and in the other tube portion the pressure is set to the saturation value corresponding to T_{test}, following the setup in [23]. The velocity of the evaporation front is computed as suggested in [65, 80] as $U_{\text{front}} = ((\rho u)_a - (\rho u)_b)/(\rho_a - \rho_b)$, where a and b refer respectively to the state after and before the evaporation wave. Averaged values are taken with results between $t = 400\,\mu$s and $t = 500\,\mu$s. Figure 7 shows the comparison between the computed and experimental values of the evaporation front velocity for the considered set of T_{test}. Good agreement is observed (similar to the results in [80]).

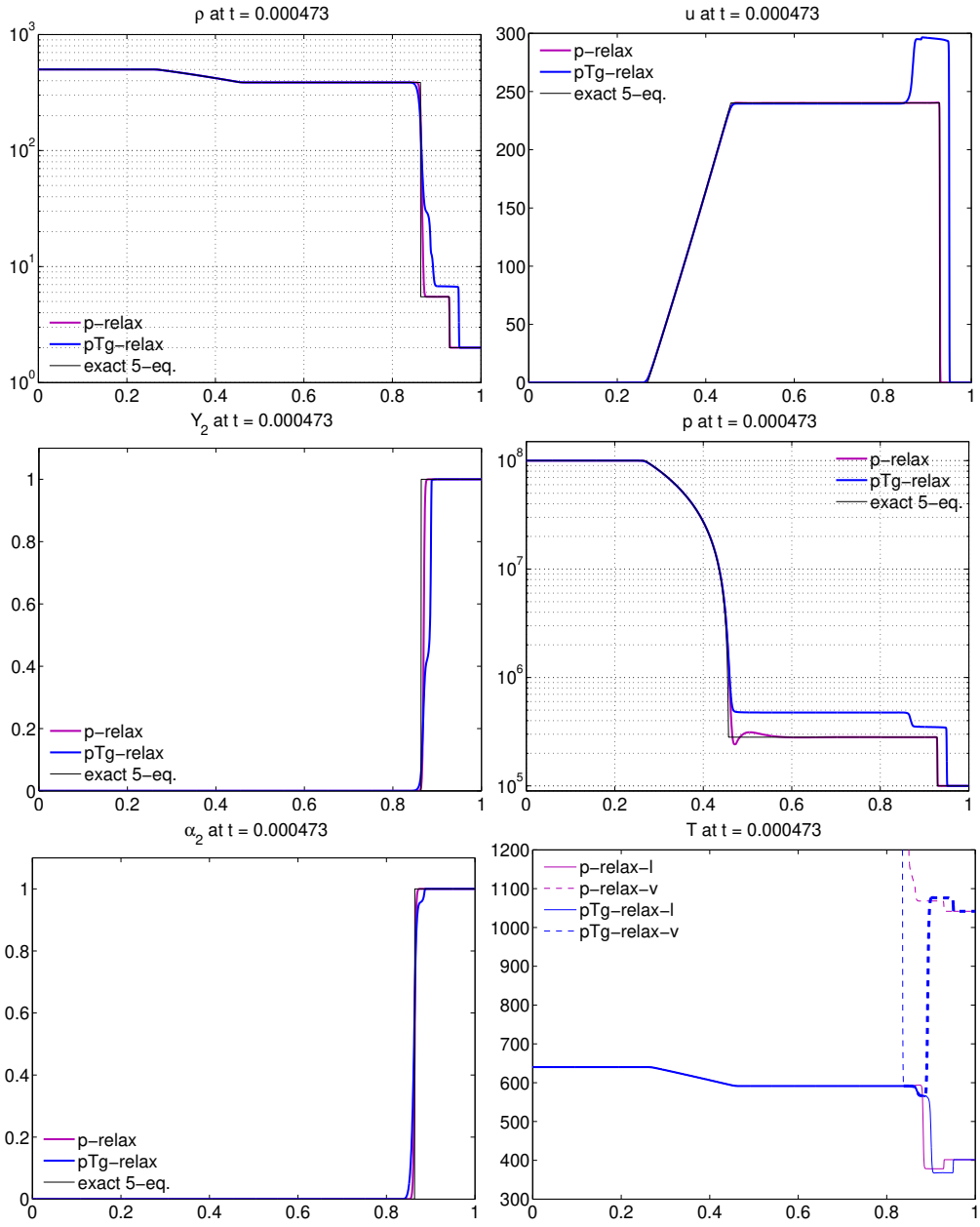

Figure 6: Dodecane shock tube test. Results at $t = 473$ μs. Density ρ, velocity u, vapor mass fraction Y_2, pressure p, vapor volume fraction α_2, vapor and liquid temperatures T_k. The density and pressure plots are in semi-logarithmic scale. p-relax (solid violet line): instantaneous mechanical relaxation; pTg-relax (solid blue line): instantaneous mechanical, thermal, and chemical relaxation. Only in the plot of the temperatures T_k the solid line indicates the liquid (l) and the dashed line the vapor (v). Moreover, for the pTg-relaxed case (blue) thinner lines indicates regions where one phase is almost absent. The exact solution of the 5-equation p-relaxed model (solid black line) is also plotted.

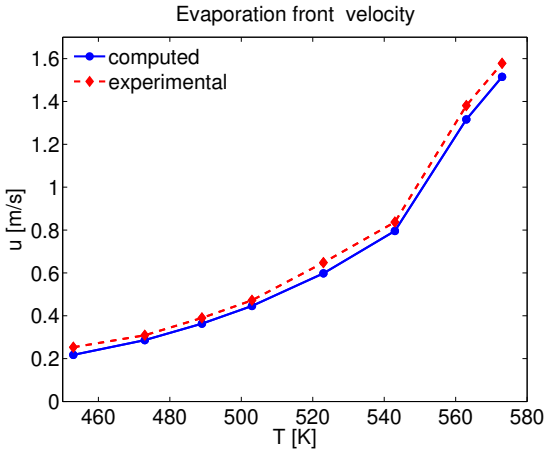

Figure 7: Comparison between computed (blue circles) and experimental (red diamonds) values of the evaporation front velocity for the set of dodecane evaporation tests performed by Simões-Moreira and Shepherd [72].

8.2.4. Barták's depressurization experiment

We simulate here the Barták's blowdown experiment presented in [5]. This laboratory experiment consists in the rapid depressurization of a pressurized water pipe initiated by a disk rupture. The study of this type of blowdown experiment is relevant in particular in the context of the hazard assessment of water-cooled reactors of nuclear power plants. One characteristic feature of the flow in this test is the rapid fall of the pressure to a value below the saturation pressure, so that for a certain time there is metastable superheated liquid, before vaporization starts. As we observe numerically, to simulate this problem it is important to be able to model non-instantaneous mass transfer processes. Initially in the tube there is liquid water at a pressure $p = 12.5 \times 10^6$ Pa and at temperature $T = T_1 = T_2 = 563.15$ K. There is an initial uniformly distributed small amount of vapor in the tube, with volume fraction $\alpha_{\text{vap}} = 10^{-3}$. The tube has a length of 1700 mm, and it is permanently closed on one side, here the right side. On the other side, here the left side, the tube is suddenly opened, hence we consider atmospheric pressure conditions at the left boundary, with $p = 10^5$ Pa. We use the NASG equation of state for water with the parameters in Table 5.

We compute solutions for this test with 1000 grid cells (CFL = 0.5) until a final time $t = 17.5$ ms (note that in this test we study the very first stage of this type of transient flow). In Figure 8 we plot results for the pressure history (left) and the vapor mass fraction history (right) at a fixed location corresponding to the first pressure gauge of the experimental apparatus, at $x = 48$ mm. The solid dark blue line represents results obtained by activating instantaneous heat transfer ($\vartheta \to \infty$) and finite-rate mass transfer with the mass transfer relaxation function ν expressed by the following relation, which is a modified version of the relations presented in [21, 16]:

$$\nu = C_r \alpha_2^{0.6} \left(\frac{p_{\text{sat}} - p}{p_{\text{crit}} - p_{\text{sat}}} \right)^{1.76}, \quad C_r = 1 \text{ Pa} \cdot \text{kg}^2/(\text{s} \cdot \text{J}^2), \tag{84}$$

where $p_{\text{crit}} = 22.0640 \cdot 10^6$ Pa. We observe the qualitative agreement of these results with the experimental data (black marks $*$), and in particular the ability of the numerical model to predict the occurrence of a metastable superheated state with $p < p_{\text{sat}}(T)$ (region of the pressure

undershoot), followed by vaporization. In Figure 8 we also plot results computed with no mass transfer ($\vartheta \to \infty$, $\nu = 0$, dashed light blue line) and results computed with instantaneous heat and mass transfer ($\vartheta \to \infty$, $\nu \to \infty$, solid red line), this being similar to a solution of the homogeneous equilibrium model (HEM) (pTg-relaxed model (24)). We notice in particular that the activation of instantaneous mass transfer does not allow the description of metastable states.

Table 5: Parameters for the NASG EOS for liquid and vapor water in the temperature range 350-550 K

phase	γ	ϖ [Pa]	η [J/kg]	$\tilde{\eta}$ [J/(Kg · K)]	κ_v [J/(Kg · K)]	b [m^3/kg]
liquid	1.387	8899×10^5	-1244191	0	3202	4.78×10^{-4}
vapor	1.954	0	2287484	6417	462	0

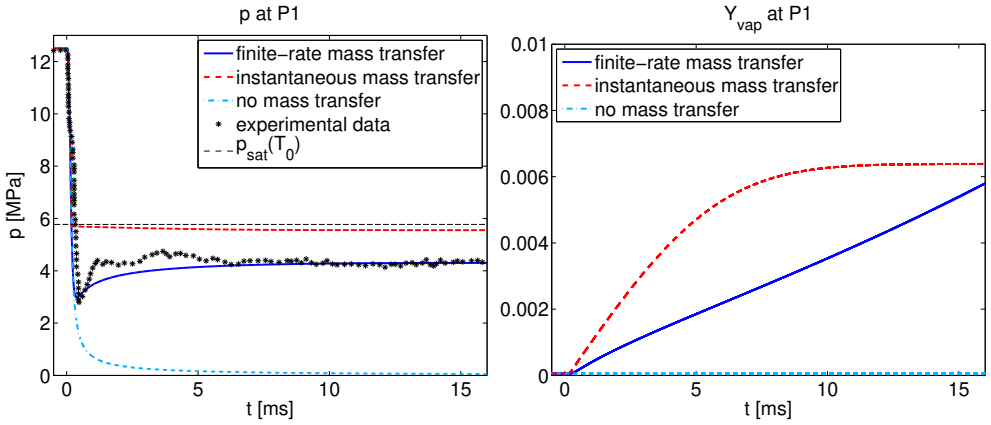

Figure 8: Barták depressurization experiment. Computed results for the pressure history (left) and vapor mass fraction history (right) at $x = 48$ mm (location of the first pressure gauge P1 in the experimental apparatus), and comparison with the experimental results of [5]. Solid blue line: finite-rate mass transfer (ν defined in (84)); dash-dot light blue line: no mass transfer; dashed red line: instantaneous mass transfer ($\nu \to \infty$), similar to a HEM solution. The value corresponding to the saturation pressure at the initial temperature $T_0 = 563.15$ K is also indicated in the left plot (dashed fine black line).

8.2.5. High-pressure fuel injector

Finally, we simulate a two-dimensional fuel injector. This test is also a variant of a test proposed in [65], which we solved in [55] with the stiffened gas equation of state and instantaneous relaxation processes. We consider a nozzle where liquid fuel (dodecane) is injected from a high-pressure tank to a chamber at atmospheric pressure. The nozzle has the shape shown in the plots of Figures 9-10, and it has a length of 10 cm and a height of 4 cm. The height of the throat is 1.2 cm, and the outer inclination angles of the converging and diverging chambers with respect to the horizontal direction are 45° and 10°, respectively. We set an initial discontinuity at $x = 0.8$ cm between a region of liquid dodecane at a pressure $p = 10^8$ Pa and at temperature $T = 550$ K and a region of dodecane vapor at pressure $p = 10^5$ and with phasic density $\rho_{\text{vap}} = 5$ kg · m^{-3}. At the initial time, a small amount of vapor is present in the liquid with $\alpha_{\text{vap}} = 10^{-4}$, and a small amount of liquid is present in the vapor with $\alpha_{\text{liq}} = 10^{-6}$. Phases are initially assumed in thermal equilibrium. The dodecane liquid and vapor phases are modeled

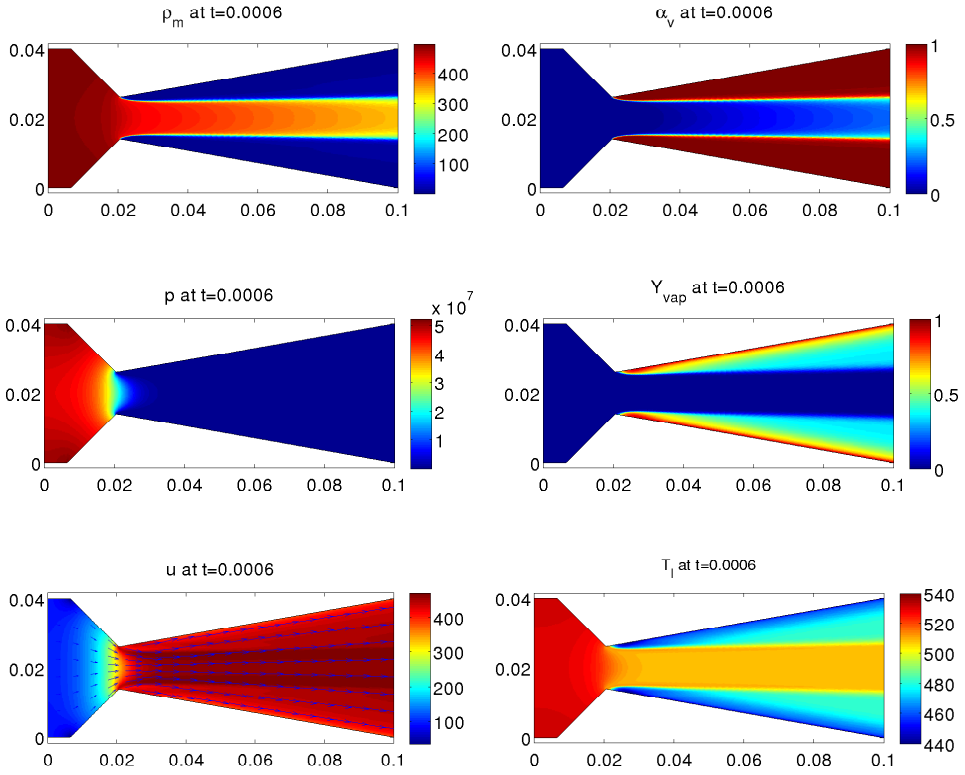

Figure 9: High-pressure fuel injector experiment. Computed results with instantaneous mass transfer for the density ρ, the vapor volume fraction α_v, the pressure p, the vapor mass fraction Y_{vap}, the velocity field u, and the liquid temperature T_l at time $t = 0.0006$ s using a 400×160 grid.

by the NASG EOS with the parameters in Table 4. In this experiment we activate instantaneous heat and mass transfer at interfaces defined by $\min(\alpha_{vap}, \alpha_{liq}) > \epsilon$, with $\epsilon = 0.9 \times 10^{-4}$. We assume instantaneous thermal relaxation ($\vartheta \to \infty$), while we use different values of the chemical relaxation parameter ν. In Figure 9 we plot results computed with instantaneous heat and mass transfer at a time at which stationary conditions are approximately attained for the mixture density, the vapor volume fraction, the pressure, the vapor mass fraction, the velocity field, and the liquid temperature. For these results we have used 400×160 grid cells and CFL number = 0.4. In Figure 10 we plot results at three different times for the vapor mass fraction computed by using four different values of the chemical relaxation parameter ν [Pa $\cdot$ kg^2/(s $\cdot$ J^2)], $\nu = 0$ (no mass transfer), $\nu = 0.1$, $\nu = 25$, $\nu \to +\infty$ (instantaneous mass transfer). For the results in this Figure 10 we have used 200×80 grid cells and CFL number = 0.4. Note that we can compare results for the vapor mass fraction at $t = 0.0006$ s obtained for the test with instantaneous mass transfer with two different mesh sizes, see Figure 9, plot at the center-right, and Figure 10, plot at the center of the bottom row. Overall the results of this numerical test show the capability of the numerical model to simulate mass transfer processes of arbitrary rate, from slow to very fast processes.

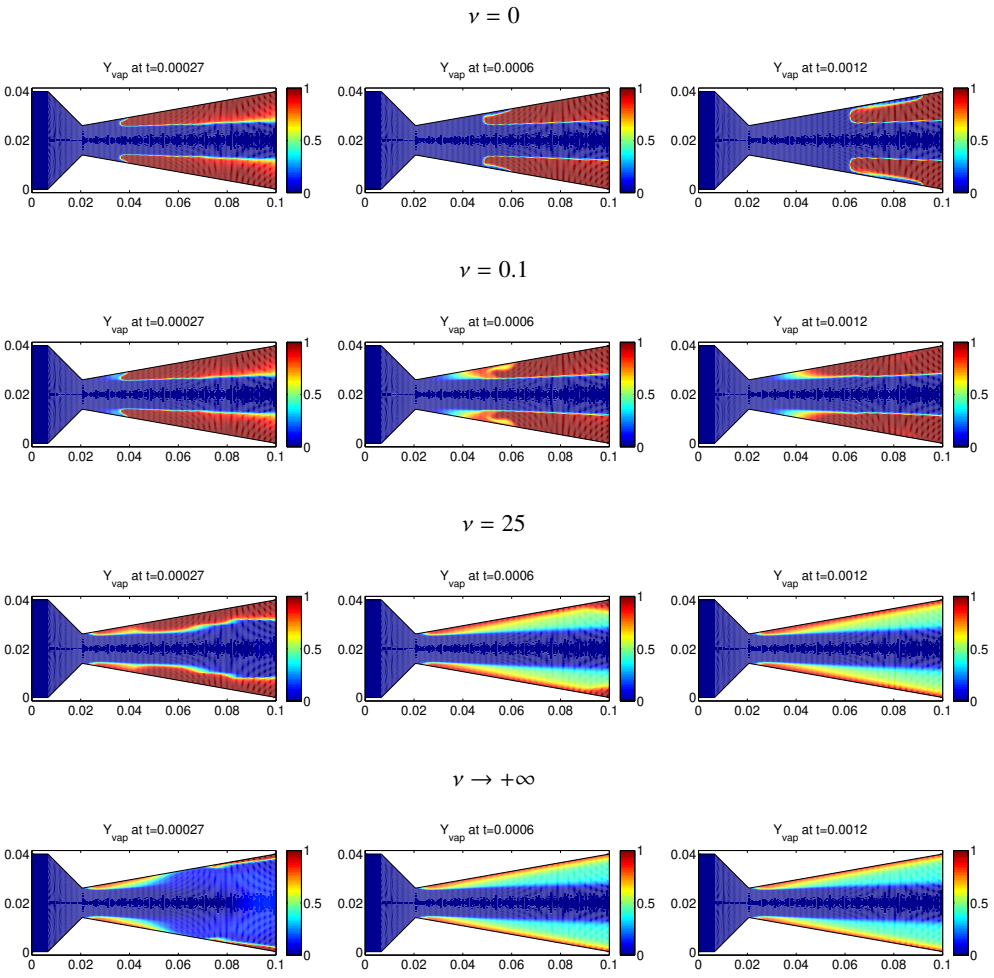

Figure 10: High-pressure fuel injector experiment. Computed vapor mass fraction Y_{vap} at times $t = 0.00027,\ 0.0006,\ 0.0012\,\text{s}$ (columns from left to right) for $\nu = 0$, $\nu = 0.1$, $\nu = 25$, $\nu \to +\infty$ (rows from top to bottom), using a 200×80 grid.

9. Conclusions

We have proposed new efficient numerical techniques to treat the mechanical, thermal, and chemical relaxation source terms of the single-velocity two-phase flow model (1) that we have presented in previous work [55]. The new techniques are based on analytical semi-exact exponential solutions of the systems of ordinary differential equations used to model the relaxation processes, and they have two significant features: the applicability to a general equation of state, and the capability to describe arbitrary-rate heat and mass transfer. These relaxation procedures also ensure a mixture-energy-consistent scheme. The procedures are simple, and for equations of state that can be written in the form of the Mie–Grüneisen EOS they do not need iterative methods. In general, for more complex equations of state, only the mixture energy equation (43) that defines implicitly the equilibrium mixture pressure might need an iterative solution method. The relaxation techniques for heat and mass transfer can robustly handle both stiff instantaneous processes and non-stiff slow finite-rate relaxation processes. This is an important improvement with respect to our previous work [17, 18]. Let us also note that, by construction, the techniques that we have proposed for the six-equation model (1) can be used to treat relaxation terms of the p-relaxed (9) and pT-relaxed (18) models, when one solves these models directly (see for instance the application to the pT-relaxed model in [20]). Several numerical tests show the effectiveness of the new relaxation techniques. We have first observed the good performance of the numerical model in problems with interfaces and strong shocks and complex equations of state. Then we have shown the ability of the methods to describe finite-rate mass transfer processes, which for instance is essential for predicting the occurrence of metastable superheated liquid in fast depressurization problems. The capability of approximating efficiently solutions to the p-relaxed and pT-relaxed models in the limit of instantaneous mechanical and thermal relaxation has been also demonstrated numerically.

Concerning future work, one objective is to couple the new relaxation techniques with a Table Look-up Method similar to the one that we have developed in [16, 18] to employ a very precise equation of state for water, the IAPWS Industrial Formulation 1997 for Water and Steam [77], for applications to two-phase flows in fast depressurizations. Moreover, we plan to extend the proposed relaxation techniques to the three-phase flow model that we have presented in [56], in particular for applications to underwater explosion problems.

Acknowledgments

The author is grateful to Keh-Ming Shyue and Marco De Lorenzo for helpful discussions. The author was supported by the French Government Directorate for Armament (Direction Générale de l'Armement, DGA) under grant N. 2018.60.0071.00.470.75.01.

A. Derivation of the p-relaxed model

In this section we derive the p-relaxed model in (9) from the two-phase model in (1). For simplicity, we shall consider the one-dimensional case $d = 1$. We follow in particular the technique of Murrone–Guillard [49] to derive the 5-equation model from the seven-equation model (see also [10]). First, we write the system (1) in one dimension in terms of the vector of primitive variables $w \in \mathbb{R}^6$ as:

$$\partial_t w + A(w)\partial_x w = \frac{1}{\tau}\Psi(w) + \Phi(w), \tag{85a}$$

where $\tau \equiv \frac{\tilde{\mu}}{\mu}$ ($\tilde{\mu}$ is an arbitrary reference quantity to non-dimensionalize μ), and

$$w = \begin{bmatrix} \alpha_1 \\ \rho_1 \\ \rho_2 \\ u \\ p_1 \\ p_2 \end{bmatrix}, \; A = \begin{bmatrix} u & 0 & 0 & 0 & 0 & 0 \\ 0 & u & 0 & \rho_1 & 0 & 0 \\ 0 & 0 & u & \rho_2 & 0 & 0 \\ \frac{p_1-p_2}{\rho} & 0 & 0 & u & \frac{\alpha_1}{\rho} & \frac{\alpha_2}{\rho} \\ 0 & 0 & 0 & \rho_1 c_1^2 & u & 0 \\ 0 & 0 & 0 & \rho_2 c_2^2 & 0 & u \end{bmatrix}, \tag{85b}$$

$$\Psi = \tilde{\mu} \begin{bmatrix} p_1 - p_2 \\ -\frac{\rho_1}{\alpha_1}(p_1 - p_2) \\ \frac{\rho_2}{\alpha_2}(p_1 - p_2) \\ 0 \\ -\frac{1}{\alpha_1}[\Gamma_1(\mathcal{E}_1 + p_1) + \chi_1\rho_1](p_1 - p_2) \\ \frac{1}{\alpha_2}[\Gamma_2(\mathcal{E}_2 + p_1) + \chi_2\rho_2](p_1 - p_2) \end{bmatrix}, \; \Phi = \begin{bmatrix} 0 \\ \frac{\mathcal{M}}{\alpha_1} \\ -\frac{\mathcal{M}}{\alpha_2} \\ 0 \\ \frac{\Gamma_1}{\alpha_1}\mathcal{Q} + (\Gamma_1 g_1 + \chi_1)\frac{\mathcal{M}}{\alpha_1} \\ -\frac{\Gamma_2}{\alpha_2}\mathcal{Q} - (\Gamma_2 g_1 + \chi_2)\frac{\mathcal{M}}{\alpha_2} \end{bmatrix}. \tag{85c}$$

We are interested in the behavior of the solutions of (85) in the limit $\tau \to 0^+$ ($\mu = \frac{1}{\tau} \to +\infty$). We expect that these solutions are close to the set $\mathfrak{U} = \{w \in \mathbb{R}^6; \Psi(w) = 0\}$. We assume that the set of equations $\Psi(w) = 0$ defines a smooth manifold of dimension L and that for any $w \in \mathfrak{U}$ we know a parameterization Ξ (the Maxwellian) from an open subset Ω of $\mathbb{R}^L$ on a neighborhood of w in $\mathfrak{U}$. For any $v \in \Omega \subset \mathbb{R}^L$ the Jacobian matrix $d\Xi_v$ is a full rank matrix, moreover, the column vectors of $d\Xi_v$ form a basis of $\ker(\Psi'(\Xi(v)))$ [49]. Now let us define the matrix $C \in \mathbb{R}^{6\times 6}$:

$$C = [d\Xi_v^1 \dots d\Xi_v^L \, V^1 \dots V^{6-L}] \tag{86}$$

where $d\Xi_v^1, \dots, d\Xi_v^L$ are the column vectors of $d\Xi_v$ and $\{V^1, \dots, V^{6-L}\}$ is a basis of the range of $\Psi'(\Xi(v))$. Based on the observations above, the matrix C is invertible. Let us now denote with P the $L \times 6$ matrix composed of the first L rows of the inverse C^{-1}. We have also the following results (see [49]):

$$P \, d\Xi_v = \mathbb{I}_L \quad \text{and} \quad P \, \Psi'(\Xi(v)) = 0, \tag{87}$$

where $\mathbb{I}_L$ denotes the $L \times L$ identity matrix. Now to obtain a reduced pressure equilibrium model we look for solutions in the form $w = \Xi(v) + \tau z$, where z is a small perturbation around the equilibrium state $\Xi(v)$. Using this into the system (85) we obtain

$$\partial_t(\Xi(v)) + A(\Xi(v))\partial_x(\Xi(v)) - \Psi'(\Xi(v))\, z = \Phi(\Xi(v)) + O(\tau). \tag{88}$$

Multiplying the above equation by P, by using (87), and by neglecting terms of order τ, we obtain the reduced model system:

$$\partial_t v + PA(\Xi(v))d\Xi_v \partial_x v = P\Phi(\Xi(v)). \tag{89}$$

In the limit of instantaneous pressure relaxation we have $p_1 = p_2$, hence the vector of the variables of the reduced pressure-relaxed model is

$$v = [\alpha_1, \rho_1, \rho_2, u, p]^{\mathrm{T}} \in \mathbb{R}^5. \tag{90}$$

Note that here $L = 5$. The equilibrium state $\Xi(v)$ is defined by:

$$\Xi : v \rightarrow \Xi(v) = [\alpha_1, \rho_1, \rho_2, u, p, p]^{\mathrm{T}} \in \mathbb{R}^6. \tag{91}$$

The Jacobian $d\Xi_v \in \mathbb{R}^{6\times5}$ of the Maxwellian is:

$$d\Xi_v = \left[\begin{array}{ccc|c} & \mathbb{I}_4 & & \begin{matrix}0\\ \vdots \\ 0\end{matrix} \\ \hline 0 & \dots & 0 & 1 \\ 0 & \dots & 0 & 1 \end{array}\right]. \tag{92}$$

A basis $V^1 \in \mathbb{R}^6$, for the range of $\Psi'(\Xi(v))$ is found as

$$V^1 = \begin{bmatrix} 1 \\ -\frac{\rho_1}{\alpha_1} \\ \frac{\rho_2}{\alpha_2} \\ 0 \\ -\frac{\rho_1}{\alpha_1}c_1^2 \\ \frac{\rho_2}{\alpha_2}c_2^2 \end{bmatrix}. \tag{93}$$

Hence we can construct the matrix $C \in \mathbb{R}^{6\times6}$ (86), compute the inverse C^{-1}, and finally obtain the matrix $P \in \mathbb{R}^{5\times6}$ by taking the first 5 rows of C^{-1}. We find:

$$P = \left[\begin{array}{ccc|cc} & & & \frac{\alpha_1\alpha_2}{D} & \frac{\alpha_1\alpha_2}{D} \\ & \mathbb{I}_4 & & -\frac{\rho_1\alpha_2}{D} & \frac{\rho_1\alpha_2}{D} \\ & & & \frac{\rho_2\alpha_1}{D} & -\frac{\rho_2\alpha_1}{D} \\ & & & 0 & 0 \\ \hline 0 & \dots & 0 & \frac{\rho_2 c_2^2\alpha_1}{D} & \frac{\rho_1 c_1^2\alpha_2}{D} \end{array}\right], \tag{94}$$

where D is given in (10). Finally, the reduced p-relaxed multiphase flow model in (9) is obtained from (89) by using the above expression of the matrix P and by evaluating the matrix A and the source term Φ in the equilibrium state $\Xi(v)$ in (91). Let us also note that we use the relations $\chi_k = c_k^2 - \Gamma_k h_k$ in the entries of Φ in (85c).

Remark. In our previous work [55] an additional source term of the form $\mathcal{M}/\rho_{\mathrm{I}}$ was written in the equation for the volume fraction α_1 of the six-equation two-phase model (1), with ρ_{I} representing an interface density. Similar to [24], this term is not included in the present model. The purpose of the term $\mathcal{M}/\rho_{\mathrm{I}}$ in [55] was to indicate the influence of the mass transfer process on the evolution of the volume fraction. Nonetheless, the rigorous derivation of the pressure-relaxed model (9) from the system (1) shown in this Appendix reveals that indeed mass transfer terms affect α_k via the pressure relaxation process, as we observe from the contribution of $\mathcal{M}$ appearing in (9a). Note that the presence of the term $\mathcal{M}/\rho_{\mathrm{I}}$ eventually does not affect the numerical model and the numerical results presented in [55] since there $\nu = 0$ or $\nu \rightarrow +\infty$, and the procedure for treating instantaneous chemical relaxation consists in imposing directly algebraic thermodynamic equilibrium conditions.

B. Source terms of the *pT*-relaxed model

We derive here the expressions (23) appearing in the mass transfer source terms of the four-equation pT-relaxed model (18) starting from the ordinary differential equations obtained from (18) for the partial densities and the mixture internal energy:

$$\partial_t(\alpha_1\rho_1) = \mathcal{M}, \tag{95a}$$

$$\partial_t(\alpha_2\rho_2) = -\mathcal{M}, \tag{95b}$$

$$\partial_t\mathcal{E} = 0\,. \tag{95c}$$

Now we determine the source terms corresponding to the equations for the volume fraction α_1, the equilibrium temperature T, and the equilibrium pressure p. To this aim, we write the transformation matrix $\frac{d\tilde{q}}{dw}$, where

$$\tilde{q} = \begin{bmatrix} \alpha_1\rho_1 \\ \alpha_2\rho_2 \\ \mathcal{E} \end{bmatrix} = \begin{bmatrix} \alpha_1\rho_1(p,T) \\ (1-\alpha_1)\rho_2(p,T) \\ \alpha_1\mathcal{E}_1(p,T) + (1-\alpha_1)\mathcal{E}_2(p,T) \end{bmatrix}, \qquad \text{and} \qquad w = \begin{bmatrix} \alpha_1 \\ T \\ p \end{bmatrix}. \tag{96}$$

We have:

$$\frac{d\tilde{q}}{dw} = \begin{bmatrix} \rho_1 & \alpha_1\phi_1 & \alpha_1\zeta_1 \\ -\rho_2 & \alpha_2\phi_2 & \alpha_2\zeta_2 \\ \mathcal{E}_1 - \mathcal{E}_2 & C_{\mathcal{E}p} & C_{\mathcal{E}T} \end{bmatrix} \tag{97}$$

where ϕ_k and ζ_k are the derivatives defined in (16) (with $T_k = T$, $p_k = p$, $k = 1, 2$) and

$$C_{\mathcal{E}p} = \alpha_1\left(\frac{\partial\mathcal{E}_1}{\partial T}\right)_p + \alpha_2\left(\frac{\partial\mathcal{E}_2}{\partial T}\right)_p, \tag{98a}$$

$$C_{\mathcal{E}T} = \alpha_1\left(\frac{\partial\mathcal{E}_1}{\partial p}\right)_T + \alpha_2\left(\frac{\partial\mathcal{E}_2}{\partial p}\right)_T. \tag{98b}$$

The system of ordinary differential equations for $w = [\alpha_1, T, p]^{\mathrm{T}}$ is then obtained as

$$\partial_t w = \left(\frac{d\tilde{q}}{dw}\right)^{-1}\begin{bmatrix} \mathcal{M} \\ -\mathcal{M} \\ 0 \end{bmatrix} = \mathcal{M}\begin{bmatrix} \mathcal{S}_\alpha \\ \mathcal{S}_T \\ \mathcal{S}_p \end{bmatrix}, \tag{99}$$

where

$$\mathcal{S}_\alpha = \frac{1}{D_T}[C_{\mathcal{E}T}(\alpha_1\phi_1 + \alpha_2\phi_2) - C_{\mathcal{E}p}(\alpha_1\zeta_1 + \alpha_2\zeta_2)], \tag{100a}$$

$$\mathcal{S}_T = \frac{1}{D_T}[C_{\mathcal{E}T}(\rho_2 - \rho_1) + (\mathcal{E}_1 - \mathcal{E}_2)(\alpha_1\zeta_1 + \alpha_2\zeta_2)], \tag{100b}$$

$$\mathcal{S}_p = \frac{1}{D_T}[C_{\mathcal{E}p}(\rho_1 - \rho_2) - (\mathcal{E}_1 - \mathcal{E}_2)(\alpha_1\phi_1 + \alpha_2\phi_2)], \tag{100c}$$

with D_T given in (23d). Note that we can write the derivatives of $\mathcal{E}_k(p_k, T_k)$ appearing in the expressions above as:

$$\left(\frac{\partial\mathcal{E}_k}{\partial T_k}\right)_{p_k} = -\frac{\chi_k}{\Gamma_k}\phi_k\,, \qquad \left(\frac{\partial\mathcal{E}_k}{\partial p_k}\right)_{T_k} = \frac{1}{\Gamma_k}\left(1 - \chi_k\zeta_k\right), \quad k = 1, 2\,. \tag{101}$$

Using this, together with $\mathcal{E}_1 - \mathcal{E}_2 = \rho_1 h_1 - \rho_2 h_2$ and $h_k = \frac{c_k^2 - \chi_k}{\Gamma_k}$, we can rewrite the numerators of (100) and we obtain the expressions reported in (23). Let us remark that the derivation illustrated above can be extended to the case of constant temperature difference $T_2 - T_1 = \Delta T$ by considering the variables associated to the phase k as functions of p and T_k and by taking for instance $w = [\alpha_1, T_1, p]^{\mathrm{T}}$, with the constraint $T_2 = T_1 + \Delta T$, ΔT = constant. Let us finally note that the derivation of the homogeneous equations for α_1, p, T and u of the four-equation pT-relaxed model (23) from the seven-equation Saurel–Abgrall model [60] in the limit of instantaneous velocity, pressure, and temperature equilibrium has been presented in [20].

C. HLLC-type Riemann solver

We detail here the simple HLLC-type Riemann solver that we use to define the fluctuations in the wave propagation scheme (44) for the one-dimensional system $\partial_t q + \partial_x f(q) + \sigma(q, \partial_x q) = 0$, $q \in \mathbb{R}^6$, as obtained by setting $\vec{u} = u$ and $\nabla = \partial_x$ in (37). We first presented this solver in [55]. Here we give more details on the derivation since the illustration of the derivation in [55] contained some imprecision (although the final formulas were correct). First, let us recall the requirements for the waves $\mathcal{W}^l$ and speeds s^l, $l = 1, \dots, \mathscr{M}$, defined by a Riemann solver for a Riemann problem with left and right data q_ℓ and q_r, respectively. The sum of the waves must be equal to the initial jump in the vector q of the system variables:

$$\Delta q \equiv q_r - q_\ell = \sum_{l=1}^{\mathscr{M}} \mathcal{W}^l. \tag{102}$$

Moreover, for any variable of the model system governed by a conservative equation the initial jump in the associated flux function must be recovered by the sum of waves multiplied by the corresponding speeds. In the considered model the conserved quantities are $\alpha_k \rho_k$, $k = 1, 2$, and ρu, therefore in order to guarantee conservation we need:

$$\Delta f^{(\xi)} \equiv f^{(\xi)}(q_r) - f^{(\xi)}(q_\ell) = \sum_{l=1}^{\mathscr{M}} s^l \mathcal{W}^{l(\xi)} \tag{103}$$

for $\xi = 2, 3, 4$, where $f^{(\xi)}$ is the ξth component of the flux vector f, and $\mathcal{W}^{l(\xi)}$ denotes the ξth component of the lth wave, $l = 1, \dots, \mathscr{M}$. It is clear that conservation of the partial densities ensures conservation of the mixture density $\rho = \sum_{k=1}^{2} \alpha_k \rho_k$. In addition, we must ensure conservation of the mixture total energy,

$$\Delta f_E \equiv f_E(q_r) - f_E(q_\ell) = \sum_{l=1}^{\mathscr{M}} s^l (\mathcal{W}^{l(5)} + \mathcal{W}^{l(6)}), \tag{104}$$

where $f_E = u(E + \sum_{k=1}^{2} \alpha_k p_k)$ is the flux function associated to the mixture total energy E. The relation (104) ensures the fulfillment of the property (42), and it is necessary for mixture-energy-consistency (but not sufficient).

The Riemann solution structure of the HLLC-type solver for the six-equation model is similar to the classical HLLC solver for the Euler equations [76, 75], and it consists of three waves $\mathcal{W}^l$, $l = 1, 2, 3$, moving at speeds

$$s^1 = S_\ell\,, \quad s^2 = S^\star\,, \quad \text{and} \quad s^3 = S_r\,, \tag{105}$$

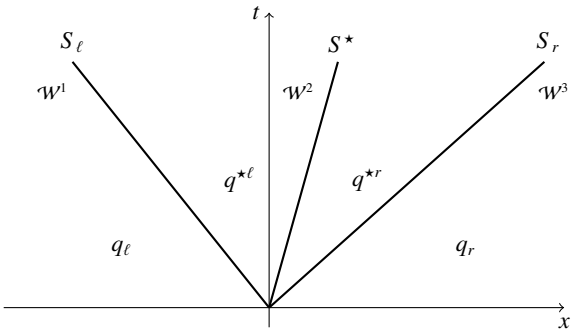

Figure 11: Solution structure of the HLLC-type solver.

which separate four constant states q_ℓ, $q^{\star\ell}$, $q^{\star r}$ and q_r (see Figure 11). In the following we will indicate with $(\cdot)_\ell$ and $(\cdot)_r$ quantities corresponding to the states q_ℓ and q_r, respectively. Moreover, we will indicate with $(\cdot)^{\star\ell}$ and $(\cdot)^{\star r}$ quantities corresponding to the states $q^{\star\ell}$ and $q^{\star r}$ adjacent, respectively on the left and on the right, to the middle wave propagating at speed $S^\star$. With this notation, the waves of the HLLC solver are

$$\mathcal{W}^1 = q^{\star\ell} - q_\ell, \quad \mathcal{W}^2 = q^{\star r} - q^{\star\ell}, \quad \text{and} \quad \mathcal{W}^3 = q_r - q^{\star r}. \tag{106}$$

Invariance conditions for the normal velocity u and for the effective pressure $p_{\rm m} = \alpha_1 p_1 + \alpha_2 p_2$, which characterize the exact Riemann solution, are imposed across the middle wave:

$$u^{\star\ell} = u^{\star r} \equiv S^\star \quad \text{and} \quad p_{\rm m}^{\star\ell} = p_{\rm m}^{\star r} \equiv p^\star\,. \tag{107}$$

Let us stress however that the single terms $\alpha_k p_k$ in general vary across this middle wave. The middle states $q^{\star\ell}$, $q^{\star r}$ are determined by imposing Rankine–Hugoniot conditions across the external waves moving at speeds S_ℓ and S_r, based on the equations for the partial densities $\alpha_k\rho_k$ and the conservative portion of the equations governing the phasic momenta $\alpha_k\rho_k u$ and the phasic total energies $\alpha_k\rho_k E_k$, $k = 1, 2$. Note that the homogeneous equations governing the phasic momenta $q_k^u = \alpha_k\rho_k u$, $k = 1, 2$, have the non-conservative form (here in one dimension):

$$\partial_t q_k^u + \partial_x f_k^u + (-1)^{k-1}\Xi(q, \partial_x q) = 0\,, \quad k = 1, 2\,, \tag{108}$$

where $f_k^u = \alpha_k\rho_k u^2 + \alpha_k p_k$ and $\Xi(q, \partial_x q) = Y_1\partial_x(\alpha_2 p_2) - Y_2\partial_x(\alpha_1 p_1) = Y_1\partial_x p_{\rm m} - \partial_x(\alpha_1 p_1) = -Y_2\partial_x p_{\rm m} + \partial_x(\alpha_2 p_2)$, as defined in (1g). Hence we impose:

$$f^{(\xi)}(q_r) - f^{(\xi)}(q^{\star r}) = S_r(q_r^{(\xi)} - q^{\star r(\xi)})\,, \quad \xi = 2, 3, 5, 6\,, \tag{109a}$$
$$f_k^u(q_r) - f_k^u(q^{\star r}) = S_r(q_{k\,r}^u - q_k^{u\,\star r})\,, \tag{109b}$$
$$f^{(\xi)}(q^{\star\ell}) - f^{(\xi)}(q_\ell) = S_\ell(q^{\star\ell(\xi)} - q_\ell^{(\xi)})\,, \quad \xi = 2, 3, 5, 6\,, \tag{109c}$$
$$f_k^u(q^{\star\ell}) - f_k^u(q_\ell) = S_\ell(q_k^{u\,\star\ell} - q_{k\,\ell}^u)\,, \tag{109d}$$

where $q^{(\xi)}$ and $f^{(\xi)}$ are the components of q and $f(q)$ (see (37b) in the $d = 1$ case). Let us remark that in writing the conditions above (109) we neglect the contribution of the non-conservative terms Ξ appearing in the phasic momentum and energy equations. We observe however that the

conditions (109) imply correct Rankine–Hugoniot conditions for the conservative equations for the mixture momentum ρu and the mixture total energy E (and hence (42) is satisfied).

The Rankine–Hugoniot conditions for the partial densities (109a) and (109c), $\xi = 2, 3$, determine the intermediate partial densities. Then the conditions for the conservative portion of the phasic momentum equations (109b) and (109d) determine the intermediate partial pressures:

$$(\alpha_k p_k)^{\star\iota} = (\alpha_k p_k)_\iota + (\alpha_k p_k)_\iota (S_\iota - u_\iota)(S^\star - u_\iota)\,, \quad \iota = \ell, r\,, \tag{110}$$

where we have also used the invariance relation for the velocity in (107). Then, using these expression in the invariance relations for the effective pressure in (107) we obtain the expression for the speed $S^\star$:

$$S^\star = \frac{p_r - p_\ell + \rho_\ell u_\ell (S_\ell - u_\ell) - \rho_r u_r (S_r - u_r)}{\rho_\ell (S_\ell - u_\ell) - \rho_r (S_r - u_r)}\,, \tag{111}$$

where we have used $p_{\mathrm{m}\ell} = p_\ell$ and $p_{\mathrm{m}r} = p_r$ since initial Riemann states are characterized by pressure equilibrium. A definition for the wave speeds must be provided, see e.g. [75, 6]. One classical and simple definition proposed by Davis [15] is

$$S_\ell = \min(u_\ell - c_{\mathrm{f}\ell}\,,\, u_r - c_{\mathrm{f}r}) \qquad \text{and} \qquad S_r = \max(u_\ell + c_{\mathrm{f}\ell}\,,\, u_r + c_{\mathrm{f}r})\,, \tag{112}$$

where c_{f} is defined in (4). Another more robust definition has been proposed for instance by Bouchut [8] (see [19]). The Rankine–Hugoniot conditions for the conservative portion of the total energy equations (109a) and (109c), $\xi = 5, 6$, together with (110) determine then the intermediate states for the total energies. Finally, we observe that the exact Riemann solution is characterized by the invariance of the volume fraction across the external waves (the volume fraction is simply advected):

$$\alpha_k^{\star\ell} = \alpha_{k\ell} \qquad \text{and} \qquad \alpha_k^{\star r} = \alpha_{kr}\,, \quad k = 1, 2\,. \tag{113}$$

Hence the solution structure for the volume fractions α_k simply consists of single jumps $\alpha_{k,r} - \alpha_{k,\ell}$ across the 2-wave moving at speed $S^\star$. As we reported in [55], the expressions for the middle states are:

$$q^{\star\iota} = \begin{pmatrix} \alpha_{1,\iota} \\ (\alpha_1\rho_1)_\iota \frac{S_\iota - u_\iota}{S_\iota - S^\star} \\ (\alpha_2\rho_2)_\iota \frac{S_\iota - u_\iota}{S_\iota - S^\star} \\ \rho_\iota \frac{S_\iota - u_\iota}{S_\iota - S^\star} S^\star \\ (\alpha_1\rho_1)_\iota \frac{S_\iota - u_\iota}{S_\iota - S^\star} \left(\frac{E_{1,\iota}}{\rho_{1,\iota}} + (S^\star - u_\iota)\left(S^\star + \frac{p_{1,\iota}}{\rho_{1,\iota}(S_\iota - u_\iota)} \right) \right) \\ (\alpha_2\rho_2)_\iota \frac{S_\iota - u_\iota}{S_\iota - S^\star} \left(\frac{E_{2,\iota}}{\rho_{2,\iota}} + (S^\star - u_\iota)\left(S^\star + \frac{p_{2,\iota}}{\rho_{2,\iota}(S_\iota - u_\iota)} \right) \right) \end{pmatrix}, \tag{114}$$

$\iota = \ell, r$. Note that in the above formulas $p_{k,\iota} = p_\iota$, $k = 1, 2$, since initial Riemann states satisfy pressure equilibrium conditions. As seen above the Rankine–Hugoniot conditions are satisfied by construction for all the physically conserved quantities across the external waves. We now also observe that Rankine–Hugoniot conditions are satisfied for the conserved quantities across the middle wave:

$$f^{(\xi)}(q^{\star r}) - f^{(\xi)}(q^{\star\ell}) = S^\star (q^{\star r(\xi)} - q^{\star\ell(\xi)})\,, \quad \xi = 2, 3, 4\,, \tag{115a}$$

$$f^E(q^{\star r}) - f^E(q^{\star\ell}) = S^\star (E^{\star r} - E^{\star\ell})\,, \tag{115b}$$

where $f^E = (E + \alpha_1 p_1 + \alpha_2 p_2)u$ is the flux function associated to the mixture total energy E. Let us remark that instead Rankine–Hugoniot conditions for the conservative portion of the equations

of the non-conserved quantities $\alpha_k\rho_k u$ and $\alpha_k E_k$ hold by construction across the external waves, but do not hold in general across the middle wave. This was inexactly reported in [55], where we incorrectly wrote Rankine–Hugoniot conditions for the phasic energies $\alpha_k E_k$ across the middle wave. As a final summarizing remark, we note that the simple HLLC-type solver illustrated here is obtained by neglecting the non-conservative term Ξ appearing in the phasic energy equations and in the phasic momentum equations in the jump conditions for the external 1-wave and 3-wave of the Riemann solution, but not for the 2-wave. The solver construction implies indeed an approximation of the non-conservative terms in the jump relations for the middle wave which can be deduced by observing:

$$f^{(4+k)}(q^{\star r}) - f^{(4+k)}(q^{\star \ell}) = ((\alpha_k E_k + \alpha_k p_k)^{\star r} - (\alpha_k E_k + \alpha_k p_k)^{\star \ell})S^{\star} \tag{116a}$$

$$= S^{\star}(q^{\star r(4+k)} - q^{\star \ell(4+k)}) + S^{\star}((\alpha_k p_k)^{\star r} - (\alpha_k p_k)^{\star \ell}), \quad k = 1, 2. \tag{116b}$$

We find that the contribution to the jump across the 2-wave representing the non-conservative term is approximated by this HLLC solver as

$$-S^{\star}((\alpha_k p_k)^{\star r} - (\alpha_k p_k)^{\star \ell}). \tag{117}$$

This is a a reasonable approximation since across the 2-wave p_{m} = constant, hence the non-conservative term Ξ in (1g) reduces to $\Xi = -\partial_x(\alpha_1 p_1)$ (and $-\Xi = \partial_x(\alpha_1 p_1) = -\partial_x(\alpha_2 p_2)$), and (117) can be then considered as a jump across the middle wave associated to the non-conservative terms $-u\partial_x(\alpha_k p_k)$, $k = 1, 2$. Let us finally remark that the simple HLLC-type that we have illustrated above belongs to a more general class of HLLC-type Riemann solvers for the six-equation two-phase flow model (37), which we have introduced and assessed in [19] by defining a Suliciu-type Riemann solver.

D. Pressure invariance at interfaces

It is well known that finite volume conservative schemes for compressible flows may produce spurious pressure oscillations at contact interfaces, as first investigated in [1]. This problem can be easily observed for multi-component flow models, however it appears also when computing single-component flows when non-linear equations of state are used. Indeed this issue is a consequence of the cell-based description of the discrete solution, together with the choice of the conserved variables as principal variables, since the pressure derived from the cell-averaged conserved quantities might differ from the uniform pressure value across contact discontinuities (see e.g. discussion in [52]). Typically the choice of pressure laws linear in the density and the internal energy per unit volume allows one to avoid difficulties. For more complex equations of state different strategies can be devised, for instance hybrid conservative/non-conservative methods or methods that introduce additional variables to be used in the pressure updating [32, 1, 2, 69, 70, 71, 51, 38]. Here we show that the pressure relaxation procedure presented in Section 7 allows us to ensure velocity and pressure invariance at material interfaces at least when the stiffened gas equation of state is used (which is linear in ρ and $\mathcal{E}$). Hence we consider here for each phase the pressure law (27) with constant parameters $\Gamma(\rho) \equiv \bar{\Gamma}$, $\varepsilon_r(\rho) \equiv \bar{\varepsilon}_r(\rho)$, $p_r(\rho) \equiv \bar{p}_r$:

$$p_k(\rho_k, \mathcal{E}_k) = \bar{\Gamma}_k(\mathcal{E}_k - \rho_k\bar{\varepsilon}_{rk}) + \bar{p}_{rk}\,. \tag{118}$$

Following [1], let us consider an isolated material interface moving in a flow with uniform velocity $\bar{u}$ and uniform pressure $\bar{p}$. For simplicity we assume $\bar{u} > 0$, but the proof below can be analogously written for $\bar{u} < 0$. We consider the one-dimensional case along the x direction.

Proposition. If at time level n we have $u_i^n = \bar{u}$ and $p_i^n = \bar{p}$, $\forall i$, then the computation by the first-order numerical scheme with instantaneous pressure relaxation (44), (57), (59) at time level $n+1$ gives $u_i^{n+1} = \bar{u}$ and $p_i^{n+1} = \bar{p}$, when the linear equation of state (118) is used for each phase.

Proof. (i) Solution of the homogeneous system by the wave propagation scheme (44). The hypothesis $u_i^n = \bar{u}$ and $p_i^n = \bar{p}$ implies that for each Riemann problem at the interface $i+1/2$ between the cells i and $i+1$ the first and third HLLC waves are $\mathcal{W}^1_{i+1/2} = \mathcal{W}^3_{i+1/2} = 0$, based on (114). Hence the HLLC Riemann solution structure at $i+1/2$ consists of a single 2-wave $\mathcal{W}^2_{i+1/2}$ moving at speed $s^2_{i+1/2} = S^\star_{i+1/2} = \bar{u}$ (based on (111)). Hence the updating formula (44) becomes (omitting here second-order corrections):

$$Q_i^{n+1} = Q_i^n - \bar{u}\frac{\Delta t}{\Delta x}(Q_i^n - Q_{i-1}^n) = (1-\xi_c)Q_i^n + \xi_c Q_{i-1}^n\,, \quad \xi_c \equiv \bar{u}\frac{\Delta t}{\Delta x}\,. \tag{119}$$

Therefore, first we easily verify

$$u_i^{n+1} = \frac{(\rho u)_i^{n+1}}{\rho_i^{n+1}} = \bar{u}\,, \quad \forall i\,. \tag{120}$$

Note that this results for the velocity invariance holds in general for any pressure law. Then we compute the phasic pressures of the homogeneous system solution step by using the equation of state above (118):

$$p_{ik}^{n+1} = \frac{1}{\alpha_{ik}^{n+1}}\left(\bar{\Gamma}_k((\alpha_k\mathcal{E}_k)_i^{n+1} - (\alpha_k\rho_k)_i^{n+1}\bar{\varepsilon}_{rk})\right) + \bar{p}_{rk} = \bar{p}\,, \quad \forall i,\ k=1,2\,. \tag{121}$$

(ii) Pressure relaxation step and pressure update. Since the solution of the homogeneous system gives $(p_1^0)_i = (p_2^0)_i = \bar{p}$ for each cell i of the computational domain, the relaxed volume fraction α_1^* (57) computed in the mechanical relaxation step is $(\alpha_1^*)_i = (\alpha_1^0)_i = (1-\xi_c)\alpha_{1,i}^n + \xi_c\alpha_{1\,i-1}^n$. Finally, the updated mixture equilibrium pressure is, based on (59) with (118):

$$p_i^{n+1} = p_i^* = \frac{\mathcal{E}_i^0 - \left((\alpha_1\rho_1)_i^0\bar{\varepsilon}_{r1} + (\alpha_2\rho_2)_i^0\bar{\varepsilon}_{r2}\right) + \left(\frac{\alpha_{1,i}^0\bar{p}_{r1}}{\bar{\Gamma}_1} + \frac{\alpha_{2,i}^0\bar{p}_{r2}}{\bar{\Gamma}_2}\right)}{\frac{\alpha_{1,i}^0}{\bar{\Gamma}_1} + \frac{\alpha_{2,i}^0}{\bar{\Gamma}_2}} \tag{122a}$$

$$= \frac{\frac{1}{\bar{\Gamma}_1}\left((1-\xi_c)\alpha_{1,i}^n\bar{p} + \xi_c\alpha_{1,i-1}^n\bar{p}\right) + \frac{1}{\bar{\Gamma}_2}\left((1-\xi_c)\alpha_{2,i}^n\bar{p} + \xi_c\alpha_{2,i-1}^n\bar{p}\right)}{\frac{1}{\bar{\Gamma}_1}\left((1-\xi_c)\alpha_{1,i}^n + \xi_c\alpha_{1,i-1}^n\right) + \frac{1}{\bar{\Gamma}_2}\left((1-\xi_c)\alpha_{2,i}^n + \xi_c\alpha_{2,i-1}^n\right)} = \bar{p}\,, \ \forall i. \tag{122b}$$

□

Although the pressure invariance is proven here only for a linear equation of state, we have observed numerically by performing numerous tests that no oscillations appear around material interfaces for more general nonlinear pressure laws of the form (27).

References

[1] R. Abgrall. How to prevent pressure oscillations in multicomponent flow calculations: A quasi conservative approach. *J. Comput. Phys.*, 125:150–160, 1996.

[2] R. Abgrall and S. Karni. Computations of compressible multifluids. *J. Comput. Phys.*, 169:594–623, 2001.

[3] P. Aursand, S. Evje, T. Flåtten, K. E. T. Giljarhus, and S. T. Munkejord. An exponential time-differencing method for monotonic relaxation systems. *Appl. Numer. Math.*, 80:1–21, 2014.
[4] M. R. Baer and J. W. Nunziato. A two-phase mixture theory for the deflagration-to-detonation transition (DDT) in reactive granular materials. *Int. J. Multiphase Flow*, 12:861–889, 1986.
[5] J. Barták. A study of rapid depressurization of hot water and the dynamics of vapour bubble generation in superheated liquid. *Int. J. Multiphase Flow*, 16(5):789–798, 1990.
[6] P. Batten, N. Clarke, C. Lambert, and D.M. Causon. On the choice of wavespeeds for the HLLC Riemann solver. *SIAM J. Sci. Comput.*, 18(6):1553–1570, 1997.
[7] Z. Bilicki and J. Kestin. Physical aspects of the relaxation model in two-phase flow. *Proc. R. Soc. Lond. A*, 428:379–397, 1990.
[8] F. Bouchut. *Nonlinear Stability of Finite Volume Methods for Hyperbolic Conservation Laws and Well-Balanced Schemes for Sources*. Birkhäuser-Verlag, 2004.
[9] S. H. Bryngelson, K. Schmidmayer, V. Coralic, J. C. Meng, K. Maeda, and T. Colonius. MFC: An open-source high-order multi-component, multi-phase, and multi-scale compressible flow solver. *Comput. Phys. Commun.*, 2020. 107396.
[10] G. Q. Chen, C. D. Levermore, and T. P. Liu. Hyperbolic conservation laws with stiff relaxation terms and entropy. *Comm. Pure Appl. Math.*, 47:787–830, 1994.
[11] A. Chiapolino, P. Boivin, and R. Saurel. A simple and fast phase transition relaxation solver for compressible multicomponent two-phase flows. *Computers and Fluids*, 150:31–45, 2017.
[12] S. Clerc. Numerical simulation of the homogeneous equilibrium model for two-phase flow. *J. Comput. Phys.*, 161:354–375, 2000.
[13] R. H. Cole. *Underwater Explosions*. Princeton University Press, 1948.
[14] F. Daude, P. Galon, Z. Gao, and E. Blaud. Numerical experiments using a HLLC-type scheme with ALE formulation for compressible two-phase flows five-equation models with phase transition. *Computers and Fluids*, 94:112–138, 2014.
[15] S. F. Davis. Simplified second-order Godunov-type methods. *SIAM J. Sci. Stat. Comput.*, 9:445–473, 1988.
[16] M. De Lorenzo, P. Lafon, M. Di Matteo, M. Pelanti, J.-M. Seynhaeve, and Y. Bartosiewicz. Homogeneous two-phase flow models and accurate steam-water table look-up method for fast transient simulations. *Int. J. Multiphase Flow*, 95:199–219, 2017.
[17] M. De Lorenzo, P. Lafon, and M. Pelanti. A hyperbolic phase-transition model with non-instantaneous EoS-independent relaxation procedures. *J. Comput. Phys.*, 379:279–308, 2019.
[18] M. De Lorenzo, P. Lafon, M. Pelanti, A. Pantano, M. Di Matteo, Y. Bartosiewicz, and J.-M. Seynhaeve. A hyperbolic phase-transition model coupled to tabulated EoS for two-phase flows in fast depressurizations. *Nucl. Eng. Des.*, 371, 2021. 110954.
[19] M. De Lorenzo, M. Pelanti, and P. Lafon. HLLC-type and path-conservative schemes for a single-velocity six-equation two-phase flow model. A comparative study. *Appl. Math. Comp.*, 333:95–117, 2018.
[20] A. D. Demou, N. Scapin, M. Pelanti, and L. Brandt. A pressure-based diffuse interface method for low-Mach multiphase flows with mass transfer. *J. Comput. Phys.*, 448, 2022. 110730.
[21] P. Downar-Zapolski, Z. Bilicki, L. Bolle, and J. Franco. The non-equilibrium relaxation model for one-dimensional flashing liquid flow. *Int. J. Multiphase Flow*, 22:473–483, 1996.
[22] E. Faucher, J.-M. Hérard, M. Barret, and C. Toulemonde. Computation of flashing flows in variable cross-section ducts. *Int. J. Comput. Fluid Dyn.*, 13:365–391, 2000.
[23] S. Fechter, C.-D. Munz, C. Rohde, and C. Zeiler. Approximate Riemann solver for compressible liquid vapor flow with phase transition and surface tension. *Computers and Fluids*, 169:169–185, 2018.
[24] T. Flåtten and H. Lund. Relaxation two-phase models and the subcharacteristic condition. *Math. Models Methods Appl. Sci.*, 21:2379–2407, 2011.
[25] D. Furfaro, R. Saurel, L. David, and F. Beauchamp. Towards sodium combustion modeling with liquid water. *J. Comput. Phys.*, 403, 2020. 109060.
[26] M. A. Gjennestad, A. Gruber, K. Y. Lervåg, Ø. Johansen, Å. Ervik, M. Hammer, and S. T. Munkejord. Computation of three-dimensional three-phase flow of carbon dioxide using a high-order WENO scheme. *J. Comput. Phys.*, 348:1–22, 2017.
[27] E. Godlewski and P.-A. Raviart. *Numerical Approximation of Hyperbolic Systems of Conservation Laws*. Springer-Verlag, New York, 1996.
[28] C. Helzel, R. J. LeVeque, and G. Warnecke. A modified fractional step method for the accurate approximation of detonation waves. *SIAM J. Sci. Comput.*, 22:1489–1510, 2000.
[29] D. M. Israel, R. L. Singleton Jr., S. W. Doebling, and J. R. Kamm. ExactPack v1.0. Los Alamos Technical Report LA-CC-14-047, 2014.
[30] K. J. Kamm. An exact, compressible one-dimensional Riemann solver for general, convex equations of state. Los Alamos Technical Report LA-UR-15-21616, 2015.

[31] A.K. Kapila, R. Menikoff, J. B. Bdzil, S. F. Son, and D.S. Stewart. Two-phase modeling of deflagration-to-detonation transition in granular materials: Reduced equations. *Physics of Fluids*, 13:3002–3024, 2001.
[32] S. Karni. Multicomponent flow calculations by a consistent primitive algorithm. *J. Comput. Phys.*, 112:31–43, 1994.
[33] O. Kunz and W. Wagner. The GERG-2008 wide-range equation of state for natural gases and other mixtures: an expansion of GERG-2004. *J. Chem. Eng. Data*, 57(11):3032–3091, 2012.
[34] S. Le Martelot, R. Saurel, and B. Nkonga. Towards the direct numerical simulation of nucleate boiling. *Int. J. Multiphase Flow*, 66:62–78, 2014.
[35] O. Le Métayer, J. Massoni, and R. Saurel. Elaborating equations of state of a liquid and its vapor for two-phase flow models. *Int. J. Therm. Sci.*, 43:265–276, 2004.
[36] O. Le Métayer, J. Massoni, and R. Saurel. Dynamic relaxation processes in compressible multiphase flows. application to evaporation phenomena. *ESAIM: Proc.*, 40:103–123, 2013.
[37] O. Le Métayer and R. Saurel. The Noble-Abel stiffened-gas equation of state. *Phys. Fluids*, 28, 2016. 046102.
[38] B. J. Lee, E. F. Toro, C. E. Castro, and N. Nikiforakis. Adaptive Osher-type scheme for the Euler equations with highly nonlinear equations of state. *J. Comput. Phys.*, 246:165–183, 2013.
[39] E. L. Lee, H. C. Horning, and J. W. Kury. Adiabatic expansion of high explosives detonation products. Lawrence Radiation Lab., University of California, Livermore, TID 4500-UCRL 50422, 1968.
[40] S. LeMartelot, B. Nkonga, and R. Saurel. Liquid and liquid-gas flows at all speeds. *J. Comput. Phys.*, 255:53–82, 2013.
[41] R. J. LeVeque. CLAWPACK. `http://www.clawpack.org`.
[42] R. J. LeVeque. Wave propagation algorithms for multi-dimensional hyperbolic systems. *J. Comput. Phys.*, 131:327–353, 1997.
[43] R. J. LeVeque. *Finite Volume Methods for Hyperbolic Problems*. Cambridge University Press, 2002.
[44] G. Linga and T. Flåtten. A hierarchy of non-equilibrium two-phase flow models. *ESAIM:ProcS*, 66:109–143, 2019.
[45] H. Lund. A hierarchy of relaxation models for two-phase flows. *SIAM J. Appl. Math.*, 72(6):1713–1741, 2012.
[46] H. Lund and P. Aursand. Two-phase flow of CO_2 with phase transfer. *Energy Procedia*, 23:246–255, 2012.
[47] R. Menikoff. Complete Mie–Grüneisen equation of state. Technical Report LA-UR-12-22592, 2016.
[48] R. Menikoff and B. J. Plohr. The Riemann problem for fluid flow of real materials. *Rev. Modern Phys.*, 61:75–130, 1989.
[49] A. Murrone and H. Guillard. A five equation reduced model for compressible two phase flow problems. *J. Comput. Phys.*, 202:664–698, 2005.
[50] A. K. Pandare, J. Waltz, and J. Bakosi. A reconstructed discontinuous Galerkin method for multi-material hydrodynamics with sharp interfaces. *Int. J. Numer. Meth. Fluids*, 92:874–898, 2020.
[51] M. Pelanti. Pressure linearization method for the computation of real fluids. In T. Hou and E. Tadmor, editors, *Hyperbolic Problems: Theory, Numerics, Applications, Proc. 9'th Intl. Conf. on Hyperbolic Problems*, pages 797–806. Springer, 2002.
[52] M. Pelanti. *Wave Propagation Algorithms for Multicomponent Compressible Flows with Applications to Volcanic Jets*. PhD thesis, University of Washington, 2005.
[53] M. Pelanti. Low Mach number preconditioning techniques for Roe-type and HLLC-type methods for a two-phase compressible flow model. *Appl. Math. Comp.*, 310:112–133, 2017.
[54] M. Pelanti and R. J. LeVeque. High-resolution finite volume methods for dusty gas jets and plumes. *SIAM J. Sci. Comput.*, 28:1335–1360, 2006.
[55] M. Pelanti and K.-M. Shyue. A mixture-energy-consistent six-equation two-phase numerical model for fluids with interfaces, cavitation and evaporation waves. *J. Comput. Phys.*, 259:331–357, 2014.
[56] M. Pelanti and K.-M. Shyue. A numerical model for multiphase liquid-vapor-gas flows with interfaces and cavitation. *Int. J. Multiphase Flow*, 113:208–230, 2019.
[57] D.-Y. Peng and D. B. Robinson. A new two-constant equation of state. *Eng. Chem. Fundam.*, 15(1):59–64, 1976.
[58] F. Petitpas, E. Franquet, R. Saurel, and O. Le Métayer. A relaxation-projection method for compressible flows. Part II: Artificial heat exchanges for multiphase shocks. *J. Comput. Phys.*, 225(2):2214–2248, 2007.
[59] M. G. Rodio and R. Abgrall. An innovative phase transition modeling for reproducing cavitation through a five-equation model and theoretical generalization to six and seven-equation models. *Int. J. Heat Mass Transf.*, 89:1386–1401, 2015.
[60] R. Saurel and R. Abgrall. A multiphase Godunov method for compressible multifluid and multiphase flows. *J. Comput. Phys.*, 150:425–467, 1999.
[61] R. Saurel, P. Boivin, and O. LeMétayer. A general formulation for cavitating, boiling and evaporating flows. *Computers and Fluids*, 128:53–64, 2016.
[62] R. Saurel, S. Gavrilyuk, and F. Renaud. A multiphase model with internal degree of freedom, application to shock-bubble interaction. *J. Fluid Mech.*, 495:283–321, 2003.
[63] R. Saurel and O. Le Métayer. A multiphase model for compressible flows with interfaces, shocks, detonation waves

and cavitation. *J. Fluid Mech.*, 431:239–271, 2001.
[64] R. Saurel and C. Pantano. Diffuse-interface capturing methods for compressible two-phase flows. *Annu. Rev. Fluid Mech.*, 50:105–130, 2018.
[65] R. Saurel, F. Petitpas, and R. Abgrall. Modelling phase transition in metastable liquids: application to cavitating and flashing flows. *J. Fluid Mech.*, 607:313–350, 2008.
[66] R. Saurel, F. Petitpas, and R. A. Berry. Simple and efficient relaxation methods for interfaces separating compressible fluids, cavitating flows and shocks in multiphase mixtures. *J. Comput. Phys.*, 228:1678–1712, 2009.
[67] K. Schmidmayer, S. H. Bryngelson, and T. Colonius. An assessment of multicomponent flow models and interface capturing schemes for spherical bubble dynamics. *J. Comput. Phys.*, 402, 2019. 109080.
[68] K. Schmidmayer, F. Petitpas, S. Le Martelot, and E. Daniel. ECOGEN: An open-source tool for multiphase, compressible, multiphysics flows. *Comput. Phys. Commun.*, 251, 2020. 107093.
[69] K.-M. Shyue. An efficient shock-capturing algorithm for compressible multicomponent problems. *J. Comput. Phys.*, 142:208–242, 1998.
[70] K.-M. Shyue. A fluid-mixture type algorithm for compressible multicomponent flow with van der Waals equation of state. *J. Comput. Phys.*, 156:43–88, 1999.
[71] K.-M. Shyue. A fluid-mixture type algorithm for compressible multicomponent flow with Mie–Grüneisen equation of state. *J. Comput. Phys.*, 171:678–707, 2001.
[72] J. R. Simões-Moreira and J. E. Shepherd. Evaporation waves in superheated dodecane. *J. Fluid Mech.*, 382:63–86, 1999.
[73] H. B. Stewart and B. Wendroff. Two-phase flow: models and methods. *J. Comput. Phys.*, 56:363–409, 1984.
[74] I. Tiselj, A. Horvat, and J. Gale. Numerical scheme of the WAHA code. *Multiph. Sci. Technol.*, 20(3-4):323–354, 2008.
[75] E. F. Toro. *Riemann Solvers and Numerical Methods for Fluid Dynamics*. Springer-Verlag, Berlin, Heidelberg, 1997.
[76] E. F. Toro, M. Spruce, and W. Speares. Restoration of the contact surface in the HLL Riemann solver. *Shock Waves*, 4:25–34, 1994.
[77] W. Wagner, J. R. Cooper, A. Dittmann, J. Kijima, H.-J. Kretzschmar, A. Kruse, R. Mareš, K. Oguchi, H. Sato, I. Stöcker, O. Šifner, Y. Takaishi, I. Tanishita, J. Trübenbach, and Th. Willkommen. The IAPWS Industrial Formulation 1997 for the Thermodynamic Properties of Water and Steam. *Transactions of the ASME*, 122:150–182, 2000.
[78] W. F. Xie, T. G. Liu, and B. C. Khoo. Application of a one-fluid model for large scale homogeneous unsteady cavitation: The modified Schmidt model. *Computers and Fluids*, 35:1177–1192, 2006.
[79] W. F. Xie, Y. L. Young, T. G. Liu, and B. C. Khoo. Dynamic response of deformable structures subjected to shock load and cavitation reload. *Comput. Mech.*, 40:667–681, 2007.
[80] A. Zein, M. Hantke, and G. Warnecke. Modeling phase transition for compressible two-phase flows applied to metastable liquids. *J. Comput. Phys.*, 229:2964–2998, 2010.